Author/s:
Ho, M;Wasko, C;O'Shea, D;Nathan, R;Vogel, E;Sharma, A

Title:
Changes in flood-associated rainfall losses under climate change

Date:
2023-10-01

Citation:
Ho, M., Wasko, C., O'Shea, D., Nathan, R., Vogel, E. & Sharma, A. (2023). Changes in flood-associated rainfall losses under climate change. Journal of Hydrology, 625, https://doi.org/10.1016/j.jhydrol.2023.129950.

Persistent Link:
https://hdl.handle.net/11343/337131

Changes in flood-associated rainfall losses under climate change

Michelle Ho[1*], Conrad Wasko[1], Declan O'Shea[1], Rory Nathan[1], Elisabeth Vogel[2,3,4], Ashish Sharma[2]

1. Department of Infrastructure Engineering, The University of Melbourne
2. Water Research Centre, School of Civil and Environmental Engineering, The University of New South Wales
3. ARC Centre of Excellence for Climate Extremes, Australia
4. Melbourne Climate Futures, The University of Melbourne

*Correspondence: m.ho@unimelb.edu.au

Abstract

Climate change is expected to impact the severity and frequency of floods, which has implications for flood risk management. Design floods and derived flood frequency curves obtained using event-based rainfall-runoff models are widely used in industry to assess flood risks for planning and design purposes. For these approaches it is necessary to have (a) rainfall inputs, and (b) rainfall losses specified, the latter representing the amount of rainfall that is either intercepted, stored on the surface, or infiltrated into the soil and does not contribute to the flood hydrograph. There is extensive research on changes in flooding under climate change that focus on projections of rainfall. However, there is little research

into projections of rainfall losses under climate change, despite the knowledge that their changes will modulate the flood response. Here, we present one of the first studies seeking to quantify how rainfall losses, as represented by estimates of initial and continuing losses for use with event-based models, are projected to change under climate change.

We identify dependencies between rainfall losses and antecedent soil moisture in around half (over 200) of the largely unregulated catchments (i.e. watersheds) in Australia analysed in this study and use these relationships to project rainfall losses under climate change. Near universal increases in both the mean and variance of both initial losses and continuing losses are projected in these catchments, suggesting that increased rainfall losses could offset the impact of increased rainfalls for frequently occurring floods and result in an increased variance in flood responses.

Keywords

Rainfall losses; event-based rainfall-runoff modelling; floods, climate change

Highlights

- Rainfall losses are a key input to event-based flood models widely used in practice
- Relationship between rainfall losses and antecedent soil moisture are quantified
- Climate change projections of soil moisture are used to project rainfall losses
- Both the magnitude and variance of future rainfall losses are projected to increase
- Climate change will affect rainfall losses and hence flood responses

1. Introduction

Anthropogenic changes to the global climate are expected to alter the hydrological cycle (IPCC, 2021). In recent decades such impacts have materialised in the changing frequencies and intensities of rainfall events (Fowler et al., 2021; Utsumi and Kim, 2022) as well as the timing and magnitude of seasonal streamflow (Barnett et al., 2008). It is widely accepted that climate change will result in increased rainfall intensities of at least 6-7% per degree of global warming (Lenderink and van Meijgaard, 2008; Liu et al., 2009; Trenberth, 2011). These projected increases in precipitation have been assumed to directly lead to increases in floods (e.g. Trenberth, 1999; Bates et al., 2008; Westra et al., 2014), however recent observations of flood magnitudes show unchanged or even decreasing floods (Lins and Slack, 1999; Blöschl et al., 2015; Do et al., 2017; Sharma et al., 2018), a dichotomy resulting from the complex nature of flood generation. The focus of these flood studies was on the processes leading to fluvial or pluvial floods in rural catchments (i.e. watersheds), and for convenience such events are herein simply referred to as “floods”.

Although floods are inherently caused by rainfall events, the magnitude of the flood response is influenced by a range of factors including the spatial and temporal distribution of the rainfall as well as catchment morphology (Pilgrim and Cordery, 1993; Johnson et al., 2016). Catchment processes prevent a portion of rainfall, collectively known as rainfall losses, from contributing to flood runoff. Rainfall losses result from 1) interception by vegetation and other surfaces; 2) depression storage on the land surface ranging in size from soil-particle-sized depressions to lakes; and 3) infiltrated water stored in the soil (Pilgrim and Cordery, 1993; Hill and Thomson, 2019; O’Shea et al., 2021). The rates at which water infiltrates into the soil profile is influenced by antecedent moisture conditions and has

consequently been shown to be a key modulator of flood responses (Pathiraja et al., 2012; Tramblay et al., 2021; Woldemeskel and Sharma, 2016; Berthet et al., 2009).

The modelling of flood responses and estimates of flood frequency have been approached using event-based models (Eagleson, 1972) and methods such as classical design storm, derived flood frequency, or joint probability approaches (Kuczera et al., 2006). Event-based models are commonly used for practical applications in flood management including engineering design (Pilgrim and Cordery, 1993; Institute of Hydrology, 1999; United States Department of Agriculture, 2014; Ball et al., 2019a) and operational flood forecasting (Lettenmaier and Wood, 1993; Coustau et al., 2013; Bahramian et al., 2021). To derive a design flood using a calibrated event-based model, it is necessary to (1) input a design rainfall; and (2) specify the loss parameters that quantify the amount of event rainfall that does appear in the direct flood response. There are limited benefits in estimating rainfall losses using complex process-based models due to challenges in representing variations in losses at fine spatial scales given the inherent errors associated with hydrological data and subsequent incomplete understanding of runoff generation processes (Pilgrim and Cordery, 1993). Hence, in practice, rainfall loss parameters are typically estimated for design flood assessments using parsimonious lumped models, such as the Soil Conservation Service Curve Number (SCS-CN), the Probability Distributed Model (PDM), and the Green and Ampt loss model. In this study we adopt the “initial loss continuing loss model” (Pilgrim and Cordery, 1993; US Army Corps of Engineers, 2000). We refer readers to O’Shea et al. (2021) for a comparison of different rainfall loss models and the implications of using each to estimate large floods.

There exists a significant body of research examining changes to rainfall under climate change and how rainfall projections may be used to inform changes to flood model inputs. For example, many studies downscale rainfall for use in continuous simulation models to estimate flood frequency under climate change (e.g. Prudhomme et al., 2002; Kwon et al., 2011), while others have developed non-stationary intensity-duration-frequency (IDF) curves using temporal trends for use in event-based models (e.g. Strupczewski et al., 2001; Hanel and Buishand, 2011; Madsen et al., 2014). Many countries now adopt change factors for their IDF curves in engineering design (e.g. Kunkel et al., 2020; and see Wasko et al., 2021b for summary of guidelines). However, despite the parameterisation of rainfall losses being a key requirement for the estimation of design floods (O'Shea et al., 2021), projections of future changes in losses, as characterised in loss models commonly used in engineering design, have yet to be quantified. That is, while we do have projections of soil moisture under climate change (e.g. Seneviratne et al., 2010; Berg et al., 2017) and such information has been used to better understand the modulating influence of antecedent conditions on floods (e.g. Brocca et al., 2009; Tramblay et al., 2010; Wasko et al., 2020), there is no direct means to relate such changes to the parameterisation of loss models used in event-based models.

A possible reason for a lack of research into climate impacts on loss model parameters may be the disparity between the spatial and temporal resolutions of climate and hydrological models. Event-based flood models are typically configured to represent processes within a catchment and rely on rainfall and streamflow data at sub-daily temporal resolutions relevant to the flood event that allow the magnitude and occurrence of peak flows to be precisely identified (Ball et al., 2019b). However, models used to produce climate change

projections, although often run using sub-hourly time steps, are parameterised to reproduce variability and change at multi-decadal time scales (Nese and Grenci, 2005). In addition, the spatial resolutions of models used in the most recent Coupled Model Inter-comparison Project are around 150 km $\times$ 150 km (Grose et al., 2020) are typically too coarse for resolving catchment-scale processes. Outputs from hydrological models using climate change inputs are therefore largely constrained to the spatial and temporal scales of the climate inputs, which are often downscaled and bias corrected (Chen et al., 2011; Wilson et al., 2022). Consequently, challenges in quantifying rainfall losses relevant to flood estimation are exacerbated when considering climate change due to the disparity in spatial and temporal resolutions required for estimating rainfall losses and those afforded in climate change projections. Specifically, the resolution of rainfall losses in climate models are inadequately resolved for the purpose of flood risk assessments. A surrogate measure of rainfall losses suitable for event-based modelling of design storms is therefore required in order to inform flood risk assessments under climate change.

To overcome some of the above challenges, the use of continuous flood simulation has been suggested in order to model the dynamic nature of antecedent catchment conditions and subsequent rainfall losses and supplement design storm approaches (Pathiraja et al., 2012; Johnson et al., 2016). Continuous flood models simulate flood responses over long time periods and retain estimates of catchment water storage. Most existing continuous flood models are focused on examining water resources (e.g. Wang et al., 2012; Krysanova and White, 2015; Frost et al., 2020; Alattar et al., 2020), with some exceptions (Wasko et al., 2023), with the subsequent trade-off being the resolution of processes relevant to flood frequency assessments. In addition, the increased complexity of continuous flood models is

130 often achieved through the representation of flood generating processes that are more
131 detailed than used in event-based models (Stephens et al., 2018), compromising the
132 reliability of flood and rainfall loss estimations at an event scale. The trade-offs between the
133 ability to estimate antecedent conditions in continuous models and better representation of
134 flood generation in event-based models has motivated efforts to combine these modelling
135 approaches (e.g. Heneker et al., 2003; Sheikh et al., 2009; Camici et al., 2011; Paquet et al.,
136 2013; Li et al., 2014; Yu et al., 2019).

137 Previous studies have demonstrated the efficacy of using antecedent conditions to improve
138 flood estimates from event-based models, with data sources including remote sensing data
139 (Sunwoo and Choi, 2017), assimilated streamflow data (Coustau et al., 2013; Bahramian et
140 al., 2022), and in situ measurements (Brocca et al., 2009), indicators (Cordery, 1970), and
141 modelled values of soil moisture (Tramblay et al., 2010; Bahramian et al., 2021). It has been
142 shown that antecedent moisture conditions will change in the future (e.g. Ivancic and Shaw,
143 2015; Ho et al., 2022) and also acknowledged that these changes should be considered in
144 design flood models (Pathiraja et al., 2012). However, to the best of the authors' knowledge,
145 there have been few studies aimed at quantifying the relationship between antecedent soil
146 moisture and rainfall losses relevant to event-based models (e.g. Cordery, 1970; Mein et al.,
147 1995) and none that have examined how rainfall losses are projected to change under
148 climate change.

149 Here, we investigate how rainfall losses may change under climate change through their
150 relationship to antecedent soil moisture simulated continuously using a separate water
151 balance model. Rainfall and runoff events occurring in 467 largely unregulated Australian
152 catchments spanning a broad range of catchment sizes and climate zones are analysed. We

calibrate rainfall losses for historical large rainfall events using available gauged rainfall and streamflow data. We then examine whether catchment-scale rainfall losses can be related to antecedent soil moisture. The existence of a quantifiable and significant relationship between event-scale rainfall losses and antecedent soil moisture provides the means for rainfall loss parameters to be adjusted when modelling climate change impacts on floods. This is relevant for application of both (deterministic) design storm approaches and in adjusting the central tendency of the loss distribution used in (stochastic) joint probability methods. In the following sections, the data and methods used to calibrate rainfall losses are outlined, the relationship between rainfall losses and antecedent soil moisture are quantified, and the extent to which changes in rainfall losses under climate change may be informed by projections of antecedent soil moisture changes is explored.

2. Data

A summary of the data sets and analyses are shown in Figure 1. Data sets are shown in italics in rounded boxes, while data processing and model calibration steps are shown in square-edged boxes. The arrows represent data processing and analysis dependencies, while the dashed grey boxes show the three key components of the study. The data are described in further detail in this section, while the methods used to process and analyse the data are described in Section 3.

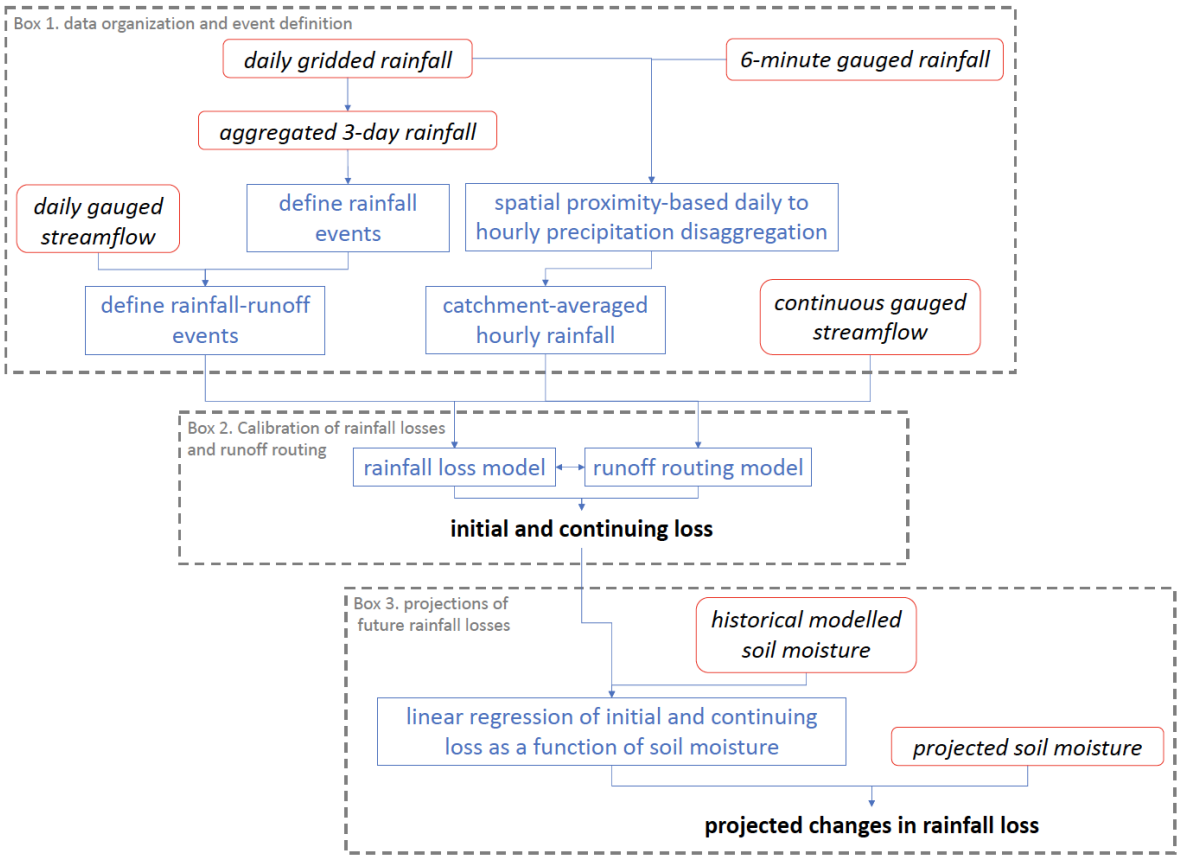

171

172 *Figure 1. Data sets (shown in italics in rounded boxes), calibration and modelling steps (shown in square-edged boxes) used*

173 *in the analysis and data outputs in bold. Dashed boxes show the three main analysis components.*

174 ## 2.1. Rainfall data

175 Daily rainfall data was sourced from the Australian Gridded Climate Data v1 (Australian

176 Bureau of Meteorology, 2020), formerly known as the Australia Water Availability Project,

177 or AWAP, dataset (Jones et al., 2009). This dataset will herein be referred to as "daily

178 gridded data". The daily gridded data are interpolated from suitable rainfall gauges ranging

179 in quantity from around 3000 to 7000 daily-read gauges over the interpolation period of

180 1900 to 2021 (Evans et al., 2020). The gauged data is interpolated to a 0.05° × 0.05°

181 latitude/longitude grid (~5 km × 5km) and a day is defined as the 24-hour period prior to

182 9 am, consistent with published daily gauged data from the Australian Bureau of

183 Meteorology (BOM). This data was then spatially averaged over each of the 467 catchments

184 considered in this study (see Section 3.1 for methods and following section for catchment
185 details) to represent catchment-scale rainfall.

186 Sub-daily rainfall data was sourced from gauged records with rainfall recorded at six-minute
187 intervals. These sub-daily rainfall records are not always located within the catchments
188 considered in this study. The gauged rainfall data was to an hourly and daily time step to
189 facilitate comparisons with, and disaggregation of, catchment-averaged-gridded rainfall
190 data from a daily to an hourly time step (see Box 1 in Figure 1). The disaggregation method
191 is described in Section 3.1 and the location of the rainfall gauges considered in this study are
192 shown in Figure 2.

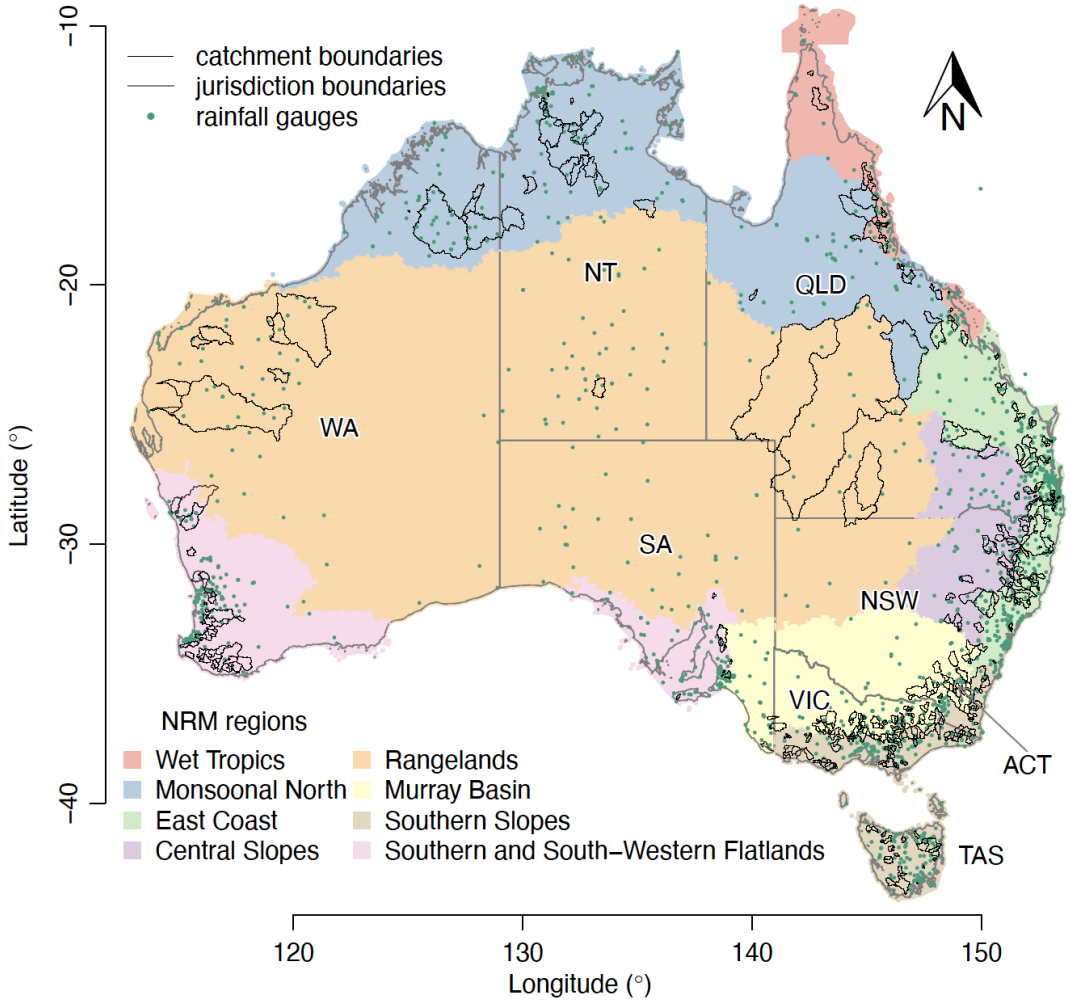

Figure 2. Location of rainfall gauges (green dots) and catchments containing a Hydrologic Reference Station (shapes with black border) within the different states and territories of Australia (ACT: Australian Capital Territory; NT: Northern Territory; NSW: New South Wales; QLD: Queensland; SA: South Australia; TAS: Tasmania; VIC: Victoria; and WA: Western Australia). Natural resource management regions (NRM in legend) are from the Department for Environment and Water (2013).

2.2. Streamflow data

Gauged volumetric streamflow records from the Hydrologic Reference Stations (HRS) are used. The HRS are a collection of streamflow gauging stations in Australia selected by the BOM using criteria based on both catchment and data quality. The HRS are located in largely unregulated catchments with minimal streamflow regulation, water extraction, and land use

change, which are deemed suitable for assessing long-term climate-induced variability and change in streamflow (BOM, 2020). The 467 catchments span regions that experience tropical, dry, and temperate climates (Peel et al., 2007), range in size from less than 10 km^2 to over 200 000 km^2 (see Figure 2), and are distributed across eight natural resource management regions, which are defined by bioregional similarity. All streamflow records in the HRS network have a minimum of 30 years of data. Missing data accounts for less than 5% of all data, has been infilled using the GR4J model (Perrin et al., 2003) and contribute to less than 10% of the total volume (BOM, 2020), while flow volumes derived by extrapolating rating curves contribute to less than 25% of the total volume. The 467 HRS used here were updated in August 2020 and are an expansion from the initial network of 222 sites previously released in 2013 (Zhang et al., 2016).

2.3. Soil moisture data

Daily soil moisture data was obtained from outputs of the Australian Water Resource Assessment Landscape modelling system (AWRA-L) version 6, a semi-distributed model used to calculate surface, shallow, and deep soil layer water stores (Frost et al., 2018). AWRA-L was developed by the BOM and the Commonwealth Scientific and Industrial Research Organisation. AWRA-L is run operationally by the BOM to inform historical assessments, seasonal forecasts, and long-term projections of water availability in Australia.

Data inputs to AWRA-L include historical temperature, daily gridded precipitation, interpolated wind speeds (from McVicar et al., 2008), and geostationary satellite-derived solar exposure data (Grant et al., 2008; Frost et al., 2018). The model simulates hydrological processes of infiltration, sub-surface storage, overland and sub-surface flows, and evaporation and evapotranspiration. Soil moisture is calculated by modelling the storage,

vertical drainage, and lateral interflow in the top, shallow, and deep soil layers based on properties of saturated hydraulic conductivity and maximum soil moisture storage. AWRA-L is run at a daily timestep, and the outputs are modelled to the same 0.05° × 0.05° latitude/longitude grid (~ 5 km× 5 km) spatial grid as the daily gridded rainfall data. The model is calibrated against gauged streamflow and satellite-derived observations of evapotranspiration and soil moisture.

The modelled outputs include the state variable of root-zone soil moisture used in this study, which is herein referred to as "soil moisture". Soil moisture is the water depth, quantified in units of mm, stored in the soil horizon 0-1 m below the surface. The ability of AWRA-L to reproduce soil moisture observations has been shown to be consistent with inferences made using remotely sensed data (Holgate et al., 2016) and is therefore deemed suitable for this analysis. Soil moisture results are presented as range-standardised soil moisture, where soil moisture measurements are divided by the catchment-specific 5^{th}-95^{th} percentile range of daily soil moisture to facilitate comparisons between catchments with different climatology and soil types.

2.4. Climate change projections

Projections of soil moisture were obtained from the BOM's National Hydrological Projections dataset (Srikanthan et al., 2022; Wilson et al., 2022). In balancing computational and storage constraints against representation of climate uncertainties, four general circulation models (GCMs) were selected to inform the National Hydrological Projections dataset (Srikanthan et al., 2022). The selection was based on 1) adequate representation of key climate features influencing the Australian climate (Moise et al., 2015); 2) adequate

249 representation of the range of uncertainty in future projections exhibited in the suite of the
250 World Climate Research Programme's Coupled Model Inter-comparison Project, Phase 5
251 (CMIP5) models; and 3) the availability of daily outputs for all variables required for running
252 AWRA-L. The four GCMs selected were ACCESS 1-0, CNRM-CM5, GFDL-ESM2M and MIROC5
253 and a single run from each GCM was used. Climate outputs from these four GCMs were
254 spatially re-gridded and bias corrected using three statistical bias corrections methods.
255 These methods were ISIMIP2b (Hempel et al., 2013), a trend preserving univariate
256 approach, a multivariate recursive nested bias-correction method (MRNBC) (Mehrotra et al.,
257 2018; Mehrotra and Sharma, 2015), and a quantile matching for extremes method (QME)
258 (Dowdy, 2019). A fourth downscaling method, referred to as CCAM-ISIMIP2b, involved
259 dynamically downscaling the GCM outputs using the regional climate model CCAM
260 (Mcgregor and Dix, 2001) and applying the ISIMIP2b method.

261 The simulations explored a baseline historical case and two climate change scenarios: one
262 scenario being representative concentration pathway 4.5 (RCP 4.5), an intermediate level of
263 mitigating greenhouse, and a scenario of very high greenhouse gas emissions (RCP 8.5).
264 These scenarios respectively correspond to radiative forcings of approximately 4.5 W/m^2
265 and > 8.5 W/m^2 in the year 2100 (Meinshausen et al., 2011; van Vuuren et al., 2011).

266 The four downscaling techniques applied to outputs from four GCMs provided 16 different
267 projections of climate for the baseline case and each of the two emission scenarios
268 considered. We refer to these downscaled and bias corrected GCM results as a 16-member
269 ensemble noting that this is in fact a four-member multi-model ensemble as bias correction
270 methods do not result in statistical independence. The small number of GCMs on which the
271 National Hydrological Projections dataset is based encompass a reasonable range of

uncertainties present in the full set of CMIP5 models. However, this ensemble is not intended for assessments of deep uncertainties in projections of climate change and such analysis is outside the scope of this study.

The projected climate variables of precipitation, temperature, wind speed, and solar exposure were used as inputs to AWRA-L to model daily soil moisture. Three 30-year time periods were evaluated. These time periods were a historical baseline period of 1976-2005 and two future periods of 2036-2065, referred to as "2050" projections, and 2070-2099, referred to as "2085" projections. For convenience, we refer to the 16-member ensemble of historical soil moisture simulated using AWRA-L forced by downscaled and bias-corrected GCM outputs as "baseline soil moisture". Similarly, the term "projected soil moisture" is used to refer to soil moisture modelled in AWRA-L using the ensemble outputs for either the 2050 or 2085 periods under scenarios of either RCP 4.5 or 8.5. The baseline and projected daily soil moisture were then spatially averaged across each of the 467 catchments containing HRS using the same method applied to the gridded rainfall data described in Section 3.1.

3. Methods

3.1. Hydroclimatic data pre-processing

Daily catchment-averaged rainfall and soil moisture were calculated for each of the catchments containing a streamflow gauge in the HRS network using the *R* package *raster* (Hijmans and van Etten, 2021). As the focus of the analysis is on the streamflow generated in response to a rainfall event, a separation of the baseflows from the direct flow response was performed using a digital filter. True values of baseflow can only be estimated with

detailed field observations (Nathan and McMahon, 1990; Ladson et al., 2013), the availability of which is limited. The application of a digital filter therefore provides a repeatable and plausible representation of baseflows and direct flows rather than an exact representation of the physical baseflow (Su et al., 2016). The recursive digital filter used here follows the methodology presented in Lyne and Hollick (1979), which has been shown to be comparable with traditional graphical techniques (Murphy et al., 2009; Nathan and McMahon, 1990) and their approximations (Sloto and Crouse, 1996; Eckhardt, 2008). The digital filter was implemented using the *hydroEvents* package in *R* (Wasko and Guo, 2022) and is formulated as:

$$Q_{d,t} = \alpha Q_{d,t-1} + \frac{1+\alpha}{2}(Q_t - Q_{t-1})$$

Equation 1

Where $Q_{d,t}$ is the direct runoff at time step t, Q_t is the total streamflow at time t, and α is the filter parameter. The filter was applied using α = 0.925, three passes for daily streamflow data (forwards from t = 1 to t = T, backwards from t = T to t = 1 and the subscript *t-1* is replaced with *t+1*, then forwards again), and nine passes for hourly data (Murphy et al., 2009). An example of the resulting baseflow separation is shown in Figure 3 (b). Unless stated otherwise, all subsequent references to streamflow refer to the direct streamflow.

3.2. Identifying rainfall runoff events

For each catchment, local maximum three-day precipitation events were identified with a minimum period of seven days between events (example shown in Figure 3 (a)). The daily three-day-aggregated time-series was calculated using catchment-averaged historical rainfall and rainfall from the GCM ensemble. The aggregation of rainfall over three days was

316 selected as it approximates the duration of mesoscale through to synoptic scale weather
317 systems (Sturman and Tapper, 1996) that are typically associated with floods in unregulated
318 catchments across a range of catchment sizes. The temporal aggregation also reduces errors
319 in identifying rainfall events that occur across the nominal daily delineation of 9 am local
320 time. A separation period of seven days was adopted between events to provide for some
321 level of independence between flood responses and approximates existing
322 recommendations based on basin areas and the timing of the onset of peak flows (Lang et
323 al., 1999; Pan et al., 2022). The seasonality of the events was examined using vector analysis
324 (Markham, 1970) where the month in which events are most frequently occurring is
325 identified and seasonality values range between 0, representing an equal distribution of
326 events across all months, and 1, where all events occur in a given month. Only rainfall
327 events larger than the 5 EY (average number of exceedances per year) were retained in the
328 analysis to provide a broad, unbiased sample of antecedent soil moisture, which are largely
329 independent from the subsequent rainfall at an event scale.

330 For each rainfall event a corresponding streamflow response was identified. A search
331 window extending two weeks prior to and 30 days after the rainfall event was used to
332 search for the start and end of each streamflow response. The start of the streamflow
333 response was identified as the nearest local flow minimum occurring either during or before
334 the rainfall event and was identified by calculating the first derivative of streamflow. The
335 start of the event was identified as the first day with rainfall greater than 1 mm occurring
336 immediately prior to the start of the streamflow response (i.e. prior to the rising limb of the
337 hydrograph). The end of the event was defined as the day when the streamflow fell below
338 7.5% of the maximum flow within the search window (Figure 3 (b)). The antecedent soil

moisture corresponding to the event was the minimum soil moisture depth occurring on either the first day or the day prior to the event. Rainfall and streamflow data over the duration of the event (shown in Figure 3 (c)) was used to calibrate the rainfall-runoff model parameters.

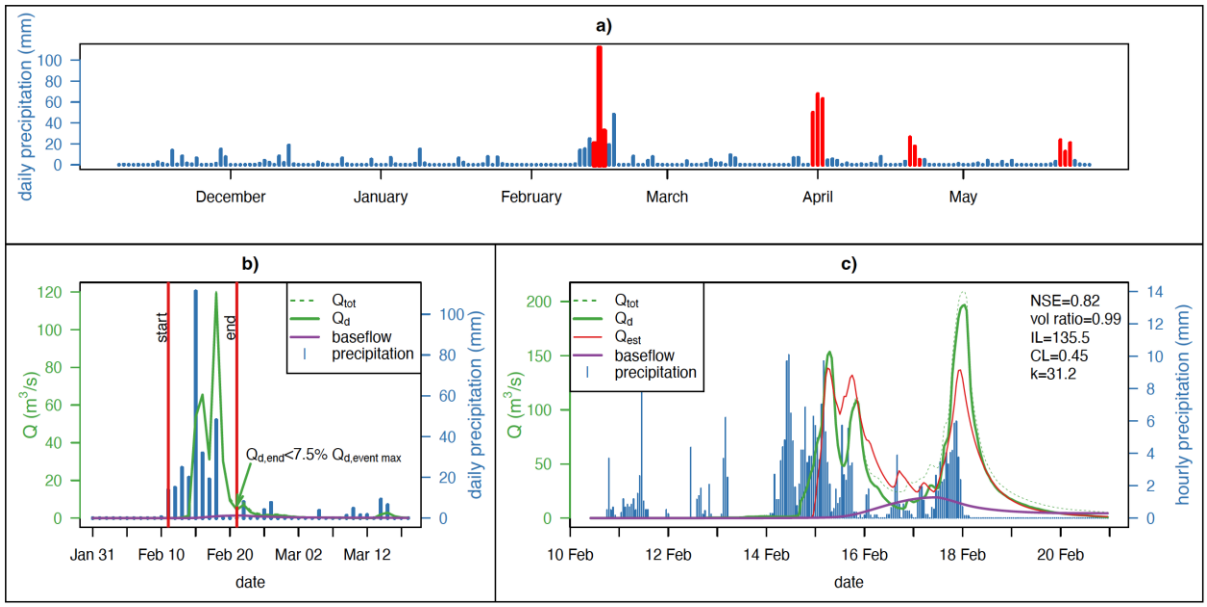

Figure 3. Schematic of a) daily precipitation (blue columns) and three-day events larger than the 5 EY (red columns – the event occurring in February appears in greater detail in b) and c)); b) the search window and definition of the start and end of the event showing the total flow rate (dotted green line), baseflow (solid purple line) and direct flow (solid green line); and c) the hourly rainfall and streamflow data used to calibrate the event, along with an estimate of the streamflow using the rainfall loss model and routing model (red line). Example data from William River at Tillegra, station number 210011.

3.3. Sub daily disaggregation

Calibrating rainfall losses requires the use of sub-daily rainfall. A proximity-based disaggregation of historical daily catchment-averaged rainfall to hourly rainfall was performed on a catchment-by-catchment basis. For each catchment a pool of candidate rainfall gauges located either within the catchment boundaries or within a 50 km radius of the catchment centroid were considered. A criterion of rainfall similarity was adopted

whereby gauges were retained if the correlation between non-zero rainfall sourced from catchment-averaged gridded rainfall data and daily-aggregated gauged rainfall data was significant at a level of $\alpha = 0.01$. A daily proportional disaggregation was then performed where daily non-zero catchment-averaged rainfall was disaggregated to hourly rainfall based on the temporal pattern recorded in the candidate gauges on the same day. Rainfall gauges were sequentially sampled in order of spatial distance from the catchment centroid to disaggregate all daily data on days where the gauged data was available. Successive rainfall gauges were used to disaggregate any remaining days of historical rainfall data.

3.4. Runoff routing and rainfall loss calibration

There are a number of loss models commonly used in event-based rainfall-runoff models (see US Army Corps of Engineers, 2000; O'Shea et al., 2021 for examples). Here, the initial loss continuing loss (ILCL) model is selected as it has been shown to be robust across a range of flood event magnitudes and in cases of extrapolation (O'Shea et al., 2021), which is germane in applications of design flood estimation. The loss model allows the storm runoff to be estimated, while the runoff routing model estimates the streamflow produced from the storm runoff and represents the lag and attenuation of storm runoff in the catchment (see Box 2 in Figure 1). Further details of the ILCL model, runoff routing model and approach to calibration is provided below.

3.4.1. Loss model

The ILCL model separates rainfall losses into two components. The initial loss represents the depth of rainfall required to sufficiently wet the catchment prior to runoff commencing. It is therefore reasonable to expect that the magnitude of the initial loss is associated with

catchment antecedent conditions. Drier catchments are expected to be associated with higher initial losses, and conversely lower initial loss values with wetter antecedent conditions. The continuing loss is a maximum rate of rainfall loss that occurs up to the end of the event once the initial loss has been satisfied. The continuing loss notionally represents the maximum infiltration capacity of the soil and may be expected to depend on catchment properties and rainfall intensity. The storm runoff, or rainfall excess X_t, at each time step *t* can be summarised as:

$$X_t = \begin{cases} 0 & \text{for } \left(\sum_{i=1}^{t} P_i\right) \leq IL \\ \max(0, P_t - CL) & \text{for } \left(\sum_{i=1}^{t} P_i\right) > IL \end{cases}$$

Equation 2

where *P* is the rainfall depth (mm) and the subscript denotes the timestep (hr), *IL* is the initial loss parameter (mm), and *CL* is the continuing loss parameter (mm/hr).

3.4.2. Rainfall-runoff routing model

For this analysis the spatially distributed catchment and channel storage characteristics within each catchment are represented by a single lumped conceptual model for routing storm runoff (X_t in Equation 2) to streamflow. Storm runoff routing is modelled using a two-parameter non-linear power-law model as follows:

$$S = kQ^m$$

Equation 3

where *S* is the total overland catchment and channel storage and *Q* is the resultant streamflow, both in units of volume in a given timestep, *k* is the routing coefficient, and *m* is the routing exponent (Pilgrim and Cordery, 1993). The value of *m* is fixed as *m* = 0.8 in accordance with general practice (Pilgrim, 1987). The value of *k* is dependent on the catchment topography, surface roughness, slope, length, and cross section of the catchments flow channels and is calibrated as described in Section 3.5.

3.5. Runoff routing and rainfall loss calibration

Two sequential calibration steps were implemented to first calibrate a catchment specific routing parameter *k* (Equation 3) and then to calibrate event-specific *IL* and *CL* parameters (Equation 2). The calibration of the parameters employed the Shuffled Complex Evolution algorithm (SCE-UA) (Duan et al., 1992), executed using the *R* package *hydromad* (Andrews and Guillaume, 2018), using rainfall and streamflow at an hourly temporal resolution to minimise objective functions that considered the Nash Sutcliffe Efficiency (NSE) and hydrograph properties.

In calibrating the catchment specific routing parameter *k*, three free parameters are first calibrated for each event: the catchment routing parameter *k*, as well as the two loss parameters *IL* and *CL*. These parameters were calibrated by using the SCE-UA to minimise the following objective function:

$$OF_k = min\left(\left|1 - \frac{\max(Q_{d,sim})}{\max(Q_{d,obs})}\right| + (1 - NSE)\right)$$

Equation 4

where OF_k is the objective function used for calibrating k, $Q_{d,sim}$ is the simulated direct streamflow, $Q_{d,obs}$ is the observed direct streamflow and NSE is the Nash Sutcliffe Efficiency, which is calculated as follows:

$$NSE = 1 - \frac{\sum_{t=1}^{t=n}\left(Q_{d,sim,t} - Q_{d,obs,t}\right)^2}{\sum_{t=1}^{t=n}\left(Q_{d,obs,t} - \overline{Q_{obs}}\right)^2}$$

Equation 5

where n is the number of hours in the event. NSE ranges in value between -∞ and 1. The objective function used for calibrating k therefore accounts for both the predictive skill of the model by considering the NSE, but in addition provides extra weight to the accuracy of the peak flow magnitude, which is often the attribute of most interest in many flood risk assessments.

Events that resulted in a poor estimation of the hydrograph after the first calibration, quantified by NSE < 0.7, were omitted and a median value of k from the remaining events was adopted as the fixed value of the routing parameter for that catchment. The fixed catchment-specific routing parameter was then used in the second calibration step, where the values of event-specific loss parameters *IL* and *CL* were optimised to minimise the following objective function:

$$OF_{loss} = min\left(\frac{\left|\sum_{t=1}^{t=n} Q_{d,sim,t} - \sum_{t=1}^{t=n} Q_{d,obs,t}\right|}{\sum_{t=1}^{t=n} Q_{d,obs,t}} + (1 - NSE)\right)$$

Equation 6

which considers the predictive skill of the model as well providing additional weight to consider the accuracy of the estimated flow volume. The optimal values of *IL* and *CL* for

435 each event are the focus of the remaining analysis where we seek to inform how these
436 parameters may shift under climate change.

437 3.6. Relating rainfall losses to antecedent soil moisture

438 At each catchment, the dependence of both initial and continuing losses on antecedent soil
439 moisture is evaluated using linear least squares regression with either *IL* or *CL* as the
440 dependent variable and antecedent soil moisture as the covariate. A significance level of
441 $\alpha = 0.05$ is adopted for assessing the significance of the slope of the linear regression. In
442 catchments where both initial and continuing loss relationships with antecedent soil
443 moisture are statistically significant, the relationships between losses and antecedent soil
444 moisture are then used to project shifts in initial and continuing losses resulting from
445 changes in soil moisture under climate change.

446 4. Results

447 4.1. Event characteristics

448 The occurrences of three-day rainfall events larger than the 5 EY were highly seasonal in
449 south-west Western Australia where winter precipitation dominates (Wright, 1974), and in
450 the Wet Tropics and Monsoonal North natural resource management regions (see Figure A.
451 1). This can be seen by the larger sized points in Figure A. 1, where seasonality values of 1
452 correspond to all events occurring within a single month and a value of 0 indicates an even
453 distribution of events throughout the year. The seasonality values of these events over the
454 rest of Australia are smaller indicating that these events occur more evenly throughout the
455 year. The Wet Tropics, Monsoonal North, East Coast, and Central Slopes regions mostly

456 experience events larger than the 5 EY event during summer whilst events are winter
457 dominated in the southern part of Australia, albeit with low seasonality in the Southern
458 Slopes and Murray Basin natural resource management regions.

459 From the selected rainfall events, the resulting streamflow responses were identified, and
460 paired rainfall and streamflow data at an hourly time step were compiled. Incomplete
461 gauged rainfall and continuous streamflow records meant that 39 catchments had
462 insufficient data (less than 3 events with complete data) with which to calibrate the event-
463 based rainfall-runoff models.

464 4.2. Historical rainfall losses

465 The runoff routing parameter *k* was first calibrated for all events prior to the calibration of
466 rainfall losses and the values are mapped in Figure A. 2. The value of *k* was shown to have
467 an approximately log-log relationship with the catchment area (see right graph in Figure A.
468 2), which is expected in natural channels where the effects of slope and surface roughness
469 compensate one another leaving catchment length as the key determinant of runoff
470 attenuation. These values were also comparable to the median routing parameter obtained
471 for the 10 largest rainfall events (Figure A. 3).

472 The catchment-specific values of *k* were then used in the second calibration step to estimate
473 event-specific *IL* and *CL* values. Results from the calibration of *IL* and *CL* at each catchment
474 were retained if adequate streamflow simulations were achieved in at least three events
475 using a criterion of NSE > 0.5. In addition to the 39 catchments previously excluded from the
476 analysis due to insufficient availability of hourly data, an additional 18 catchments were
477 excluded due to poor simulation of historical flood responses as measured by a failure to

meet the criteria of NSE > 0.7 in the calibration of *k* (see crosses located in the map in Figure A. 2) or a criteria of NSE > 0.5 for the calibration of *IL* and *CL*. Half of the catchments located in arid climate regions (17 out of 34) were excluded due to these criteria. With the exception of climate region, the excluded catchments showed little difference in catchment characteristics (e.g. catchment size, data quality) suggesting that model or data processing approaches used here are inadequate for representing the complexities of these catchments. A summary of calibrated losses across catchments within each region is shown in Figure 4 for the remaining 410 catchments. Median catchment initial loss values ranged from 6.6 mm to 114.8 mm, while the range of initial losses across all events ranged from 0-465 mm across all catchments.

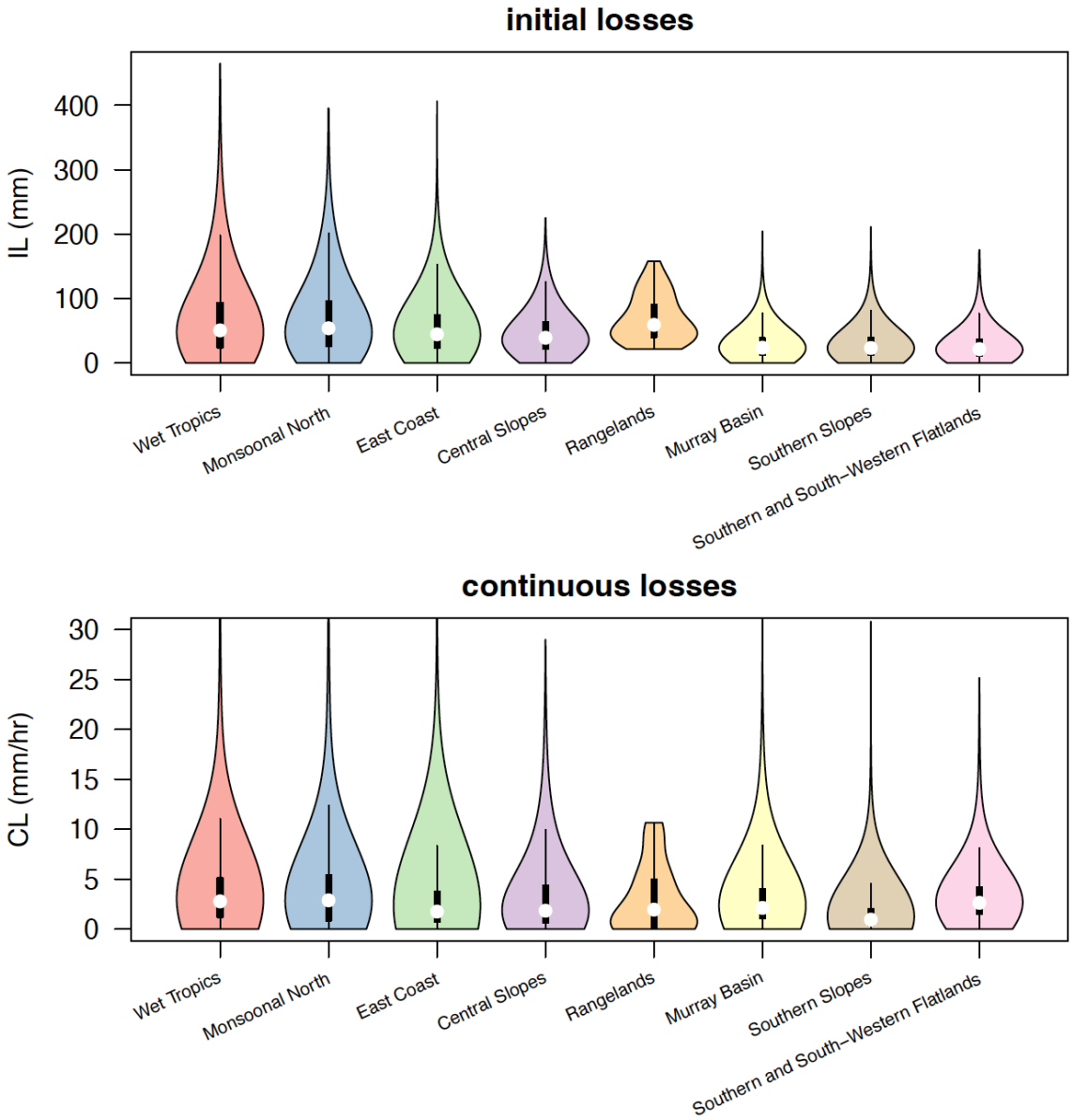

Figure 4. Violin plots of the initial loss and continuous loss across all adequately calibrated events grouped by natural resource management region, with the white dot showing the median value, thick black bars showing in the interquartile range, thin black bars show 1.5 × the interquartile range, and the shaded regions show the kernel density distribution of the loss values.

Initial losses were smaller for catchments located in the Murray Basin, Southern Slopes, and Southern and South-Western Flatlands (see Figure 4), almost all of which experience temperate climates. In these three regions the median initial losses were around 21-24 mm. These results suggest that the initial losses are lower in catchments that experience temperate climates and relatively even distributions of selected rainfall events between

498 seasons, which are likely to result in relatively wetter antecedent catchment conditions. In
499 contrast, the Central Slopes and Rangeland regions experience relatively large initial losses
500 with median initial losses of 40 and 60 mm respectively. These two regions are
501 characterised by low rainfall of less than approximately 600 mm per year and therefore
502 large initial losses may be indicative of regularly dry antecedent catchment conditions. In a
503 seeming contradiction, initial losses are also large in the Wet Tropics, Monsoonal North, and
504 East Coast regions, where average annual rainfalls exceed 600 mm. However, the
505 occurrence of rainfall events larger than the 5 EY in these regions is highly seasonal. The
506 majority of rainfall in the region occurs during the tropical wet season, a six-month period
507 between October and April. Within the wet season, rainfall is highly cyclic and typically
508 follows an approximate 50 day cycle characterised by low rainfall periods spanning 10-40
509 days (Suppiah, 1992; Wheeler et al., 2009). The occurrence of rainfall after extended dry
510 seasons, or dry periods, and associated dry antecedent catchment conditions are a plausible
511 reason for such high initial losses, which is evident in the relatively large range of initial
512 losses experienced in these regions.

513 Median catchment continuous loss values ranged from around 0-11.7 mm/hr. While these
514 values appear small, the total rainfall loss due to continuing losses is often comparable to
515 the initial loss since continuing losses occur over the duration of the storm following the
516 commencement of runoff. Median continuous losses in some regions were three times
517 those of others (e.g. 2.9 mm/hr in the Monsoonal North compared with 0.9 mm/hr in the
518 southern slopes). While ranges of initial losses could be loosely categorised by climate
519 zones, continuing losses appear to be independent of climate, with large variability in
520 continuing losses seen between catchments within the same region. This result is not

surprising, as continuing losses are expected to be influenced by endogenous catchment characteristics, and they also reflect the influence of gauging and other errors in the estimation procedure.

The variability of continuing loss values within each region is evident in the Southern and South-Western Flatlands, where the median continuing loss for catchments located in western portion of this region is 2.7 mm/hr, around 75% larger than the median continuing loss of 1.5 mm/hr in the remaining catchments in the Southern and South-Western Flatlands. It is conceivable that the difference is partly influenced by the variations in the hydraulic conductivity of the soils. For example, upper soil saturated hydraulic conductivity ranges between 150-480 mm/hr (classified as high to extreme; McKenzie et al., 2000) and 32-425 mm/hr for the subsoil for catchments located in south-west Western Australia within the Southern and South-Western Flatlands region. In comparison, the saturated hydraulic conductivity ranges between 7-157 mm/hr in the upper soil (classified as slow to high conductivity) and 1.5-60 mm/hr in the sub soil for the remaining catchments in the Southern and South-Western Flatlands region. The correlation between the saturated soil hydraulic conductivity (either topsoil or subsoil) and the median continuing loss of each catchment is significant at a level of $\alpha = 0.01$. However, the variance explained is small with less than 4% of the variance in the median continuing loss explained by either the upper soil or subsoil saturated hydraulic conductivity (see Figure A. 4 for scatter plots of median continuing loss against soil saturated hydraulic conductivity).

4.3. Relating rainfall losses to antecedent soil moisture

The dependence of event losses on antecedent soil moisture, as determined using a linear regression, is shown in Figure 5. Black points (n = 57) show locations where data availability was insufficient, or the calibration of the parameters (routing parameter, *k*, initial loss, and continuing loss) resulted in less than three events meeting the calibration standard of NSE > 0.5. The linear regression coefficient is negative for around 90% of stations for both IL and CL. The coefficient is mapped for all catchment locations recognising the somewhat arbitrary nature of selecting a significance level (e.g. Amrhein et al., 2019; Papalexiou and Montanari, 2019) where smaller plotting points are adopted for catchments where the slope is not significant at a level of $\alpha = 0.05$.

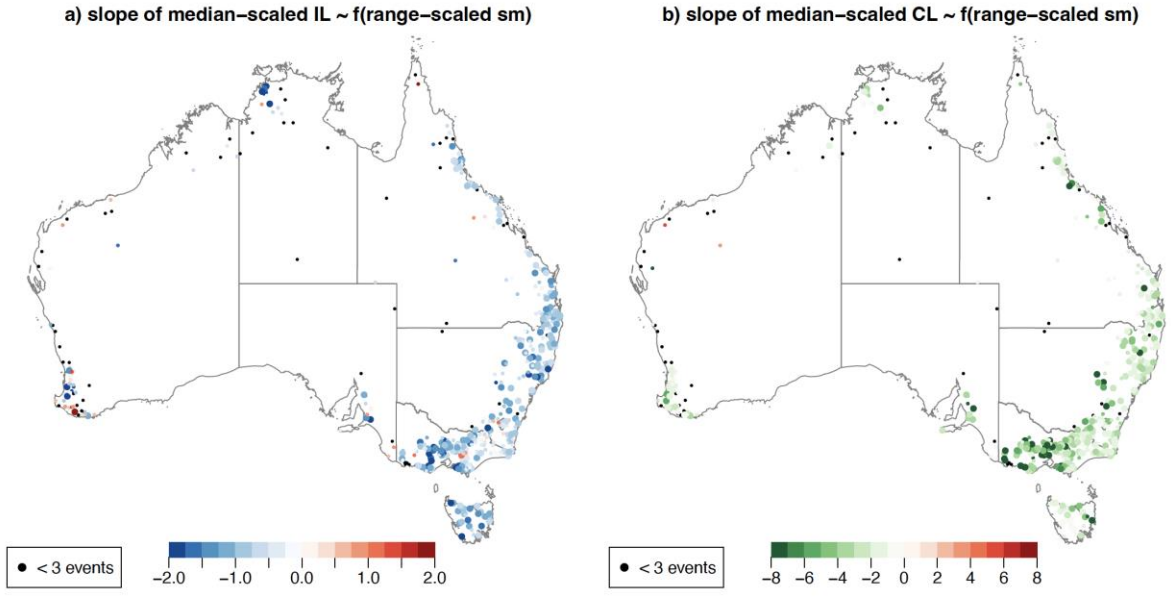

Figure 5. Values of the linear regression slope relating (a) initial loss and (b) continuing loss to the covariate of soil moisture. Losses are scaled by the catchment-specific median loss and soil moisture is scaled by the catchment-specific historical 5th-95th percentile to provide results that are comparable across locations. Smaller black points show catchments with insufficient data, while smaller coloured points show locations where results are insignificant at a $\alpha = 0.05$ level.

Significant relationships between initial loss and antecedent soil moisture are found in 207 catchments (Figure 5 (a)). These 207 catchments are spatially distributed across all regions excluding the Rangelands, with a higher density of catchments along the east coast of Australia and in the Southern Slopes region. Of these 207 significant relationships, 205 show a negative relationship between initial loss and antecedent soil moisture. Similarly, continuing losses were found to exhibit a negative relationship with antecedent soil moisture at all 273 locations with statistically significant relationships (Figure 5 (b)). The direction of this relationship is expected as drier antecedent conditions (i.e., lower soil moisture) results in higher moisture deficits and, logically, subsequent increased capacity in the catchment to absorb rainfall.

A significant positive relationship between initial loss and antecedent soil moisture was only found in two catchments and these were derived from a relatively small number of events (< 20) compared with the remaining catchments (an average of over 80 events). The 205 catchments exhibiting a significant negative relationship between antecedent soil moisture and initial loss were retained for further analysis. Similarly, all 273 locations showing significant relationships between antecedent soil moisture and continuing loss were retained for assessing climate change impacts.

Overall, the data for catchments where the relationship between rainfall losses and antecedent soil moisture were statistically insignificant was relatively scarce and on average contained around half the number of events compared to the remaining catchments. A majority of catchments located in arid climate regions also did not show a statistically significant relationship (15 out of 17). In addition, although the size of the catchments where the relationships were insignificant were larger, there did not appear to be a

579 threshold size at which the relationship between antecedent soil moisture and rainfall
580 losses becomes invalid.

581 4.4. Inferring changes in rainfall losses under climate change

582 A comparison of historical and baseline antecedent soil moisture was first made to ensure
583 that baseline representations of soil moisture in the ensemble were suitable for further use.
584 Baseline soil moisture values are slightly underestimated in the Southern Rangelands, Wet
585 Tropics and Monsoonal North regions and slightly overestimated in the East Coast and
586 Central Slopes region (Figure A. 5). However, on a continental scale, the biases in either the
587 mean or standard deviation of baseline projections of soil moisture are small (see Figure A.
588 6).

589 Projections of changes in both the initial and continuing loss relative to the baseline values
590 were respectively made for the 205 and 273 retained catchments using antecedent soil
591 moisture as the covariate (see Figure A. 7 to Figure A. 10 for projections of range-
592 standardised soil moisture from each ensemble member under RCP 4.5 and 8.5 scenarios
593 for the 2050 and 2085 time periods). The projections of shifts in losses were made for
594 locations where the dependence on soil moisture was found to be significant and negatively
595 correlated. A summary of the median changes in initial loss and continuing loss is shown in
596 Figure 6 and Figure 7 respectively.

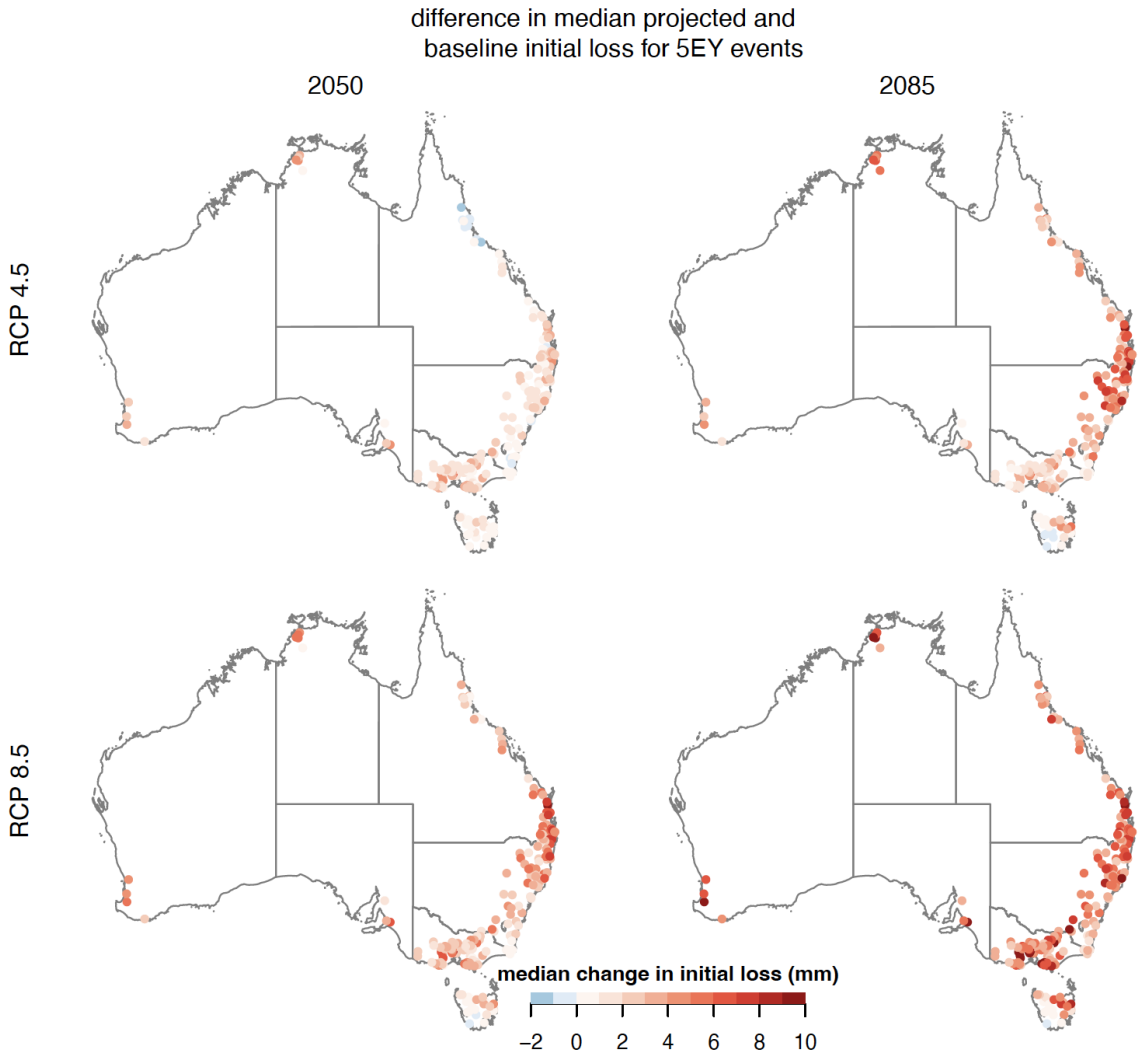

Figure 6. median change in initial loss from the baseline period (1976-2005) to the 30 years centred on (left) 2050 and (right) 2085 under the scenarios of (top) RCP 4.5 and (bottom) RCP 8.5.

Under RCP 4.5 in 2050 initial losses increase on average by 1.5 mm (3%) with an interquartile range of 0.6 to 2.2 mm (1%-5%). Initial losses are projected to increase further under RCP 8.5 in 2085 with average initial losses of 5.0 mm (9%) with an interquartile range of 3.3 to 6.3 mm (6%-12%). Initial losses are projected to increase across almost all catchments under both scenarios and for both time periods (Figure 6). There are two exceptions to these near-spatially-uniform increases in projected initial losses: south-west Tasmania, where projected decreases in initial losses are small; and a small region in north-eastern Australia, where initial losses are projected to decrease under RCP 4.5 in the 30

608 years centred on 2050. However, these losses in north-eastern Australia are projected to
609 increase in line with the majority of Australia further into the future under RCP 4.5 as well as
610 under the higher emission scenario of RCP 8.5.

611 Projected changes in continuing losses follow a similar spatial pattern to projected changes
612 in initial loss, which is expected given that antecedent soil moisture is the covariate in both
613 cases. Like initial losses, larger increases in continuing losses are seen further into the future
614 and under the scenario of higher emissions. The average increase in continuing loss is
615 0.15 mm/hr (4%) under RCP 4.5 in 2050 with an interquartile range of 0.03 to 0.23 mm/hr
616 (1%-8%). These continuing losses are larger under RCP 8.5 in 2085 with an average increase
617 of 0.45 mm/hr (13%) with an interquartile range of 0.18 to 0.63 mm/hr (8%-23%). Increases
618 in continuing losses of up to 2.7 mm/hr are projected under a climate change scenario of
619 RCP 8.5 in the 30-year period centred around 2085. The physical manifestation of increases
620 in both initial and continuing losses is a decrease in the proportion of rainfall converting to
621 runoff but upper limits of losses would be physically constrained by the hydraulic
622 conductivity of the soils limiting the infiltration capacity throughout the event.

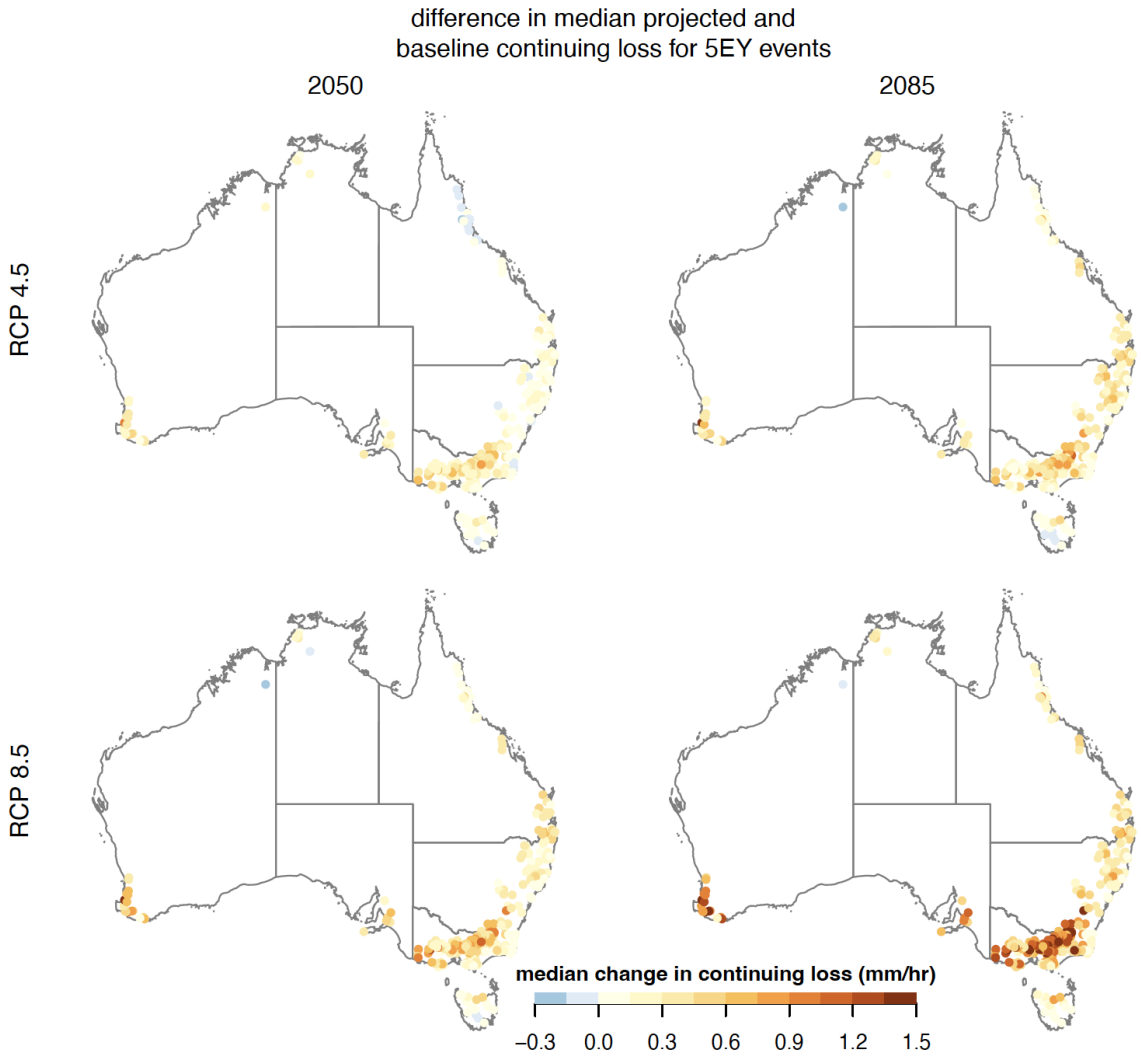

Figure 7. As for Figure 6 but for continuing loss.

The degree of error seen between the historical and baseline projections of soil moisture standard deviation (see Figure A. 6) suggest that changes in the distribution of losses may also be projected. The projected future percentage changes in the variance in initial and continuing losses are shown in Figure 8 and Figure 9 respectively. The variances in both initial and continuing loss increases across most of Australia except for south-west western Australian and inland south-east Australia, where the variance in losses is projected to decrease slightly. The largest increases in variance are seen in western Tasmania and the central East Coast regions around the border between Queensland and New South Wales. Increased variance in losses across most of Australia would result in increased variability in

flood responses under climate change. Increased variance in rainfall losses would compound the changes in floods resulting from projections of increased rainfall variability, which is particularly pronounced for precipitation extremes in arid regions (Kim et al., 2020).

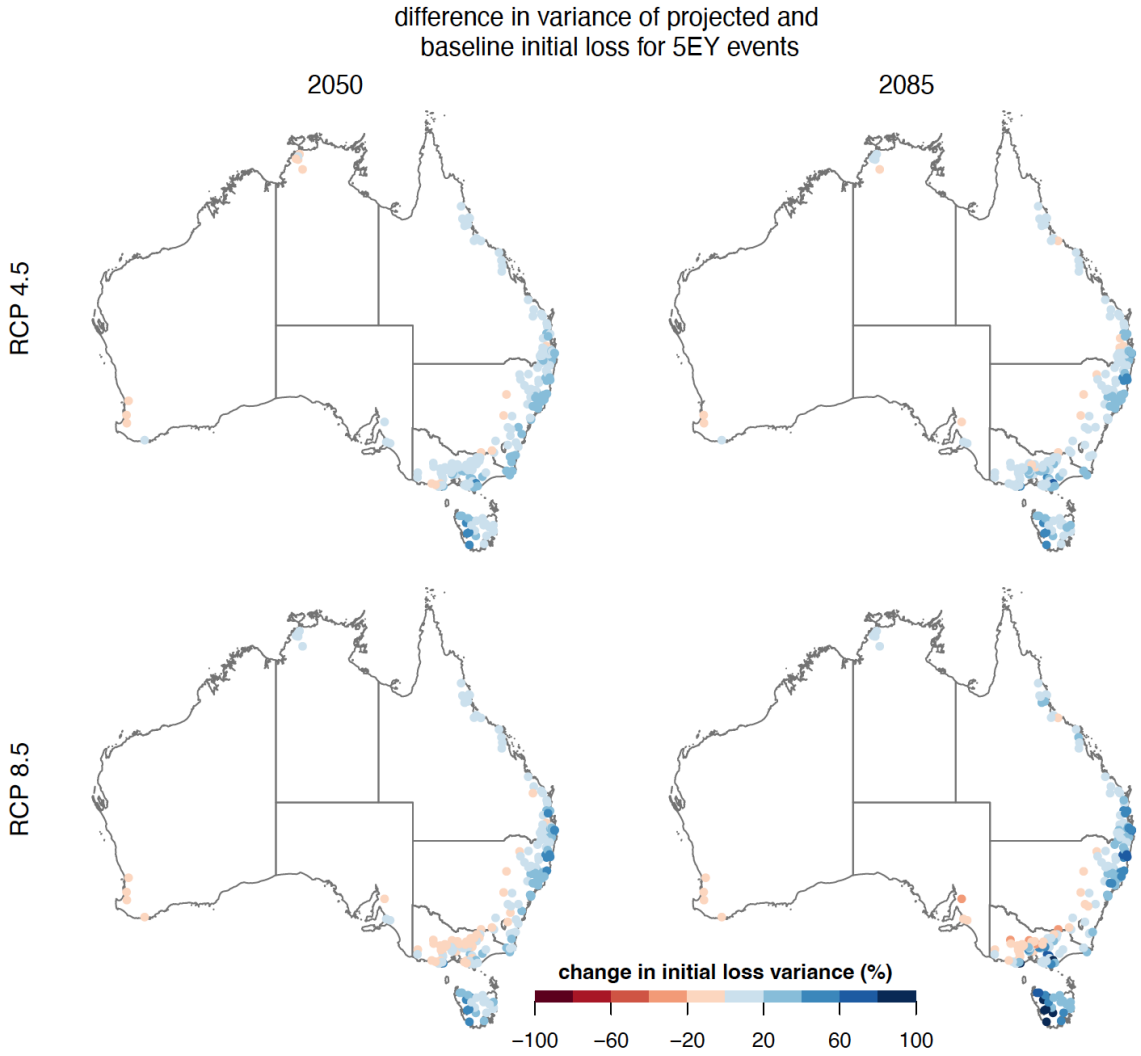

Figure 8. change in the variance of initial loss from the baseline period (1976-2005) to the 30 years centred on (left) 2050 and (right) 2085 under the scenarios of (top) RCP 4.5 and (bottom) RCP 8.5.

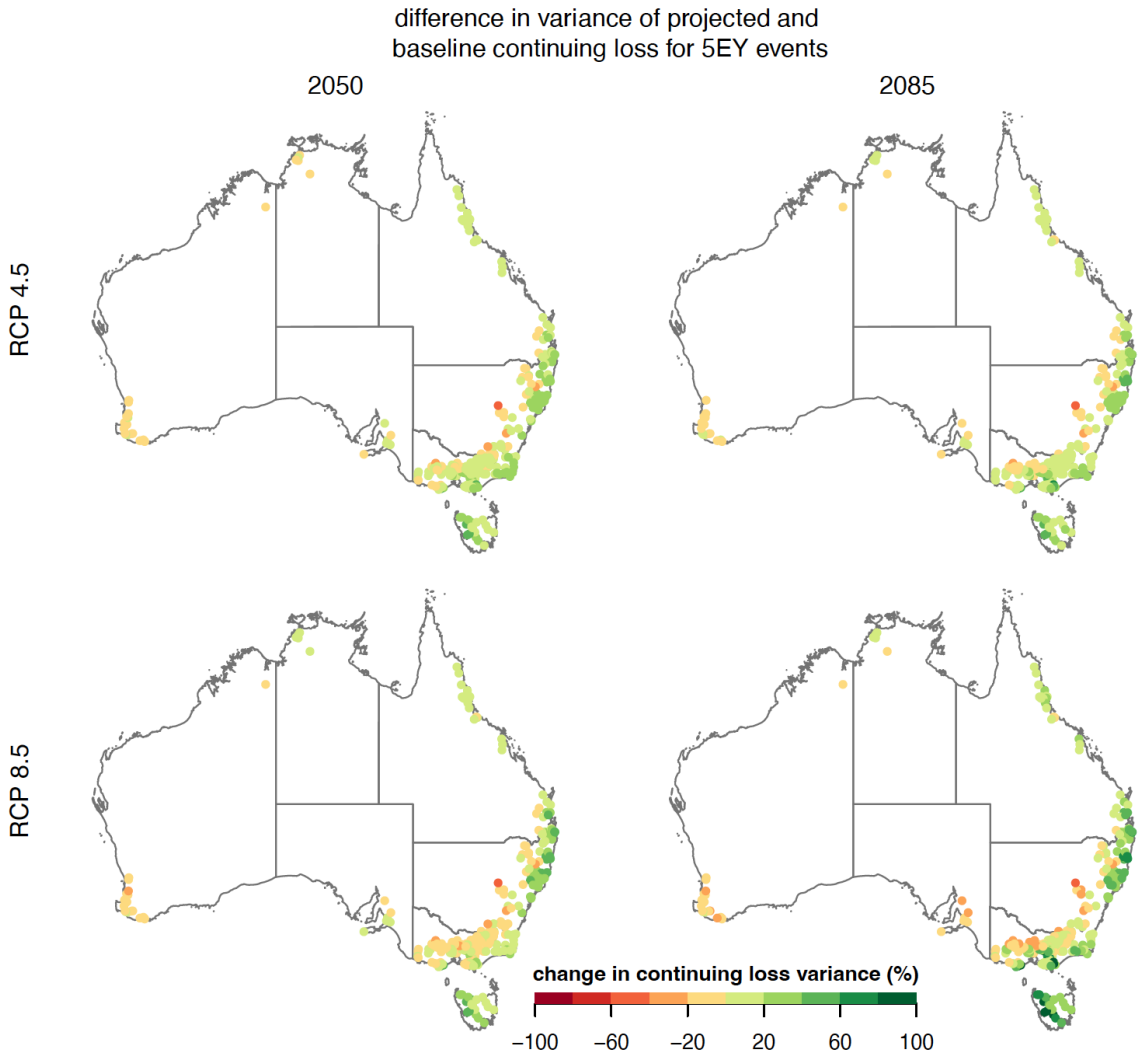

Figure 9. As for Figure 8 but for continuing loss.

5. Discussion

The provision of climate information tailored to practical applications assessing climate change impacts is essential for informing risk assessments and for developing robust adaptations (Kiem et al., 2014). Quantifying how rainfall losses are projected to change under climate change is critical given the broad use of design flood and derived flood frequency approaches in industry applications. In addition, event-based rainfall-runoff models provide the opportunity to estimate the entire flood hydrograph (Kjeldsen, 2007) yielding broader insights into the impacts of climate change on floods (e.g. on the shape and

volume of flood hydrographs) compared with existing assessments of projected changes in flood peaks (Ishak et al., 2013) or flood volumes (Ho et al., 2022) in isolation.

We discuss the implications of our findings that the magnitude and variance of rainfall losses are predominantly projected to increase in the future. Some of the additional factors needed to inform event-based models for evaluating flood runoff under climate change are outlined below. We also discuss the constraints associated with the analysis presented in this study as well as avenues for future research.

5.1. Implications of projected changes in rainfall losses

This study has focused on quantifying changes in rainfall losses under climate change for unregulated catchments in Australia. The results are location-specific and are dependent on both the climatology and catchment morphology. However, the method is applicable to any location where relationships between antecedent soil moisture and rainfall losses can be adequately quantified and would be relevant for regions where design floods and derived flood frequency curves are obtained using event-based models. Projecting changes in rainfall losses is a critical step in modelling floods under climate change as historical changes in soil moisture have been shown to impact the timing and magnitude of peak flows as well as total flood volumes (e.g. Brocca et al., 2009; Tramblay et al., 2010; Coustau et al., 2013; Wasko and Nathan, 2019; Wasko et al., 2020). Increases in losses due to climate change means that possible increases in rainfalls may be offset by drier soils meaning not all floods increase at the same rate as the rainfall, a result previously detailed by Sharma et al. (2018) and consistent with the findings of Wasko and Nathan (2019) and Wasko et al. (2023) respectively based on observed and modelled flood data. Furthermore, the results indicate that the variability in rainfall losses will increase across most locations, which will

673 exacerbate the increased variability in floods resulting from changes in rainfall extremes
674 under climate change (Wasko et al., 2021a).

675 The impacts of changing rainfall losses on flood runoff are more pronounced at lower
676 rainfall intensities (Smith et al., 2013) where a larger proportion of the total rainfall is
677 needed to satisfy the catchment moisture deficit. The impact of rising temperatures on
678 decreased soil moisture across many regions of the world has largely appeared to have
679 outweighed concurrent increases in rainfall intensity resulting in decreased peak flows
680 (Wasko et al., 2021a). Such results are indicative of increased rainfall losses and the
681 methods presented here could be used to quantify the role that changes in rainfall losses
682 have on floods globally. This apparent dichotomy between increased rainfall intensity and
683 decreased flood runoff becomes less apparent for larger, more extreme rainfall events
684 (Bennett et al., 2018). Our results are consistent with studies showing projected decreases
685 in water supply across Australia despite increases in extreme rainfall, leading to overall
686 reductions in runoff (Henley et al., 2019; Nguyen et al., 2020). The consideration of changes
687 in rainfall losses and interactions with other flood factors are therefore key considerations
688 for understanding flood responses under climate change.

689 The *relative* influences of rainfall losses on floods are also modulated by other factors such
690 as catchment size, storm characteristics, and regional climatology. For example, floods in
691 larger catchments are more sensitive to changes in rainfall losses where runoff is attenuated
692 over a larger area. Consequently, extreme rainfall events are less likely to cause extreme
693 flooding in larger catchments compared with smaller catchments (Ivancic and Shaw, 2015).
694 Flood peaks are also amplified by the interaction of the storm with the catchment. For
695 example, temporally front-loaded storms (Visser et al., submitted to Journal of Climate) and

spatial contraction of storms (Wang and Kotamarthi, 2015; Wasko et al., 2016; Peleg et al., 2018) will magnify flood peaks. In addition, flood risks in large catchments are largely driven by macro-scale storms (e.g. cyclones and fronts), while meso-scale storms (e.g. thunderstorms) are more relevant to flood risk in smaller catchments (Wright et al., 2014). Changes in event frequency and duration influenced by shifts in storm tracks (Priestley and Catto, 2022) will likewise affect antecedent moisture conditions and subsequent flood responses. Revising the inputs into event-based models that reflect these changes in storm characteristics will be necessary for assessing flood responses under climate change.

5.2. Limitations of current study

The parsimonious loss model integrates a range of both epistemic data and parameter errors as well as aleatory errors associated with the natural variability inherent in floods. In this study, hourly rainfall patterns at a catchment scale were scaled from gauged records based on spatial proximity and data availability. Consequently, some rainfall patterns were informed by rainfall gauges located outside, and at times distant to, the catchment boundary. However, ensuring the availability of rainfall observations within every catchment is not a panacea as the spatial variability of rainfall within catchments also has a significant impact on runoff generation and the temporal pattern of rainfall at a single gauge may not represent that of the whole catchment.

The mismatch in temporal resolution also applies to the daily antecedent soil moisture compared with the hourly resolution of the estimated loss parameters. Consequently, the antecedent soil moisture values may not accurately relate to the rainfall losses, but they do provide an adequate representation of the initial soil moisture state. Furthermore, the projection of rainfall losses is contingent on the validity of downscaled and bias corrected

719 rainfall from GCMs and subsequent representation of daily soil moisture to which rainfall
720 losses are related.

721 The conceptualisation of the ILCL model is based on initial losses representing the rainfall
722 needed to satisfy the catchment moisture deficit and the expectation that continuing losses
723 will largely depend on catchment characteristics such as soil hydraulic conductivity. In
724 theory, this should result in calibrated values of continuing loss that are constant. However,
725 fixed values of continuing loss would be expected only when soils are near saturated (Saul,
726 1997) or under conditions of Hortonian runoff for constant rates of rainfall. Constant rates
727 of continuing loss would therefore be expected for catchments where all runoff is generated
728 under saturation excess overflow mechanisms. It is possible that the variability in continuing
729 loss values is indicative of Hortonian (i.e. infiltration excess) runoff mechanisms being the
730 likely runoff generating mechanisms for the events examined in this study. Alternatively,
731 this variability may reflect the difficulty of representing spatially complex runoff
732 mechanisms with simple lumped conceptual models for losses.

733 Catchment-scale-aggregations of runoff generation result in an amalgamation of different
734 runoff mechanisms. For example, Hortonian runoff, saturation runoff, and infiltration
735 throughflow from varying proportions of the catchment will almost certainly be occurring
736 simultaneously within a catchment depending on factors including rainfall intensity and
737 spatial distribution, and variations in soil profiles and topographies, all of which is
738 aggregated in the estimations of rainfall losses. As a result, we find that both initial losses
739 and continuing losses vary with antecedent soil moisture, but that other (unquantified)
740 factors also contribute to the observed variability in behaviour, which impact on the degree
741 of variance that may be explained by antecedent soil moisture.

742 Despite the limitations of the ILCL model, the results demonstrate a quantifiable
743 dependence of rainfall losses on antecedent soil moisture. The relationship between soil
744 moisture and initial and continuing loss across several hundred catchments across Australia
745 enables projections of the impacts of climate change on the hourly flood generation
746 processes to be estimated. The results demonstrate that soil moisture is a statistically
747 significant predictor of rainfall losses for over half of the catchments considered (207
748 catchments for IL and 273 for CL) and may be used to inform projected changes in terms of
749 both the central tendency and dispersion of rainfall loss distributions.

750 While the ILCL rainfall loss model examined in this study is commonly used by practitioners,
751 we recognise that other event loss models are also used. Assessing the impact of climate
752 change using these other models might prove more difficult than it is for the ILCL model
753 because of the differences in model structure. For example, in the SCS-CN model, the Curve
754 Number (CN) parameter controls the volume of rainfall lost after the initial abstraction
755 (conceptually equivalent to the initial loss) is satisfied, but unlike the CL parameter, CN is
756 not clearly defined as the amount of loss occurring and this may confound attempts to
757 project changes in the CN parameter under future climates. We suspect a similar problem
758 may exist with the PDM model commonly used in the UK (Kjeldsen, 2007), where the C_{max}
759 parameter controls the volume of loss after initial loss is satisfied. These differences in
760 model structure were found by O'Shea (2021) to lead to less robust predictions under
761 extrapolation compared with the ILCL model, suggesting that the ILCL model may be more
762 suitable for assessing climate change impacts compared with other commonly used loss
763 models. The extent to which this might be true is a topic for future research.

5.3. Future research

Initial and continuing loss values are required as inputs for design storm analysis methods and could be used to inform the central tendency of losses in event-based modelling that is widely used for the design of infrastructure and flood protection works, floodplain planning and management. A negative relationship between antecedent soil moisture and both initial and continuing losses was found to be near universal across the continent. To provide information on changes in losses across a wider region or the whole of Australia, a regionalisation of the results presented in this study is needed. However, the magnitudes of the dependence on soil-moisture showed little regional clustering. Initial attempts at calibrating regional relationships of losses dependent on soil moisture clustered by natural resource management regions resulted in statistically significant relationships, but with low levels of variance explained (1%-13%) and are therefore not shown. Avenues for regionalising the relationship between rainfall losses and antecedent soil moisture could partially pool catchments based on attributes other than the natural resource management regions trialled here. The pooling of information could be achieved using hierarchical clustering or Bayesian methods (Devineni et al., 2013; Sun et al., 2015; Ho et al., 2017).

Event-based rainfall-runoff models may be used in probabilistic frameworks by sampling the distributions of select model inputs within a Monte Carlo framework (Rahman et al., 2002; Kuczera et al., 2006; Nathan et al., 2002). Implementing a Monte Carlo framework requires exogenous specification of the model input distributions. Our results suggest that it may be possible to specify changes in the location and variance of both initial and continuing losses under climate change that negate the use of more complicated combined continuous and event-based modelling approaches (Camici et al., 2014).

6. Conclusions

The use of event-based rainfall-runoff models to derive design floods or flood frequency curves is a widely used approach in engineering design and floodplain management and underpins flood estimation guidelines in many different countries. The critical nature of floods coupled with a changing risk profile resulting from climate change emphasises the importance of, and motivates the need for, studies that tailor climate projections suitable for use in event-based rainfall-runoff models. The selection of design rainfalls and rainfall losses are two key assumptions used in event-based models for estimating design floods. While numerous studies have sought to inform how climate change will impact rainfall, there is a dearth of studies aimed at resolving how rainfall losses, as they are used in practice, will be impacted by climate change, despite the recognition that antecedent conditions and subsequent rainfall losses have significant influence over the flood response. In this study we have identified catchments in Australia where rainfall losses can be related to soil moisture, a catchment variable exhibiting long system memory that is well modelled in continuous water balance simulations. Using this relationship, we have been able to provide projections of how rainfall losses, which impact flood responses at a sub-daily time scale, may change under decadal-scale climate change. While our results are location specific, our methods for identifying dependencies between soil moisture and rainfall losses suitable for projecting losses under climate change are globally applicable. Both initial and continuing losses are projected to near-universally increase across Australia into the future. Initial losses are on average projected to increase 9% with increases of up to 30% for some catchments under the highest emissions scenario. Similarly, continuing losses are projected to increase 13% on average under the highest emissions scenario, with increases of up 55%

for some catchments. Rainfall losses comprise but one component of design storm, derived flood frequency, or joint probability approaches to flood frequency estimation and ongoing examinations of changes in other factors affecting floods at an event scale are needed to provide a sound basis for future assessments of floods under climate change.

Acknowledgments

The HRS streamflow data set is publicly available from www.bom.gov.au/hrs. Gridded rainfall from AGDC is accessible from the National Computational Infrastructure via registered access. Sub-daily rainfall data is available for a cost from the Australian Bureau of Meteorology or from the authors at reasonable request. Gridded AWRA-L soil moisture is freely available upon request from http://www.bom.gov.au/water/landscape/

The authors thank Carly Tozer for the discussions around climate change impacts on rainfall.

This project was supported the Australian Research Council (ARC) Discovery Projects DP200101326, DE210100479. Michelle Ho is funded by a collaboration jointly funded by the Department of Natural Resources, Mine and Energy, HydroElectric Corporation, Melbourne Water Corporation, Murray-Darling Basin Authority, Seqwater, Snowy Hydro, SunWater, Water Corporation (Western Australia) and WaterNSW. Declan O'Shea acknowledges the support of an Australian Government Research Training Program Scholarship and the University of Melbourne Lochrie Engineering Scholarship.

References

Alattar, M.H., Troy, T.J., Russo, T.A., Boyce, S.E., 2020. Modeling the surface water and groundwater budgets of the US using MODFLOW-OWHM. Advances in Water Resources 143, 103682. https://doi.org/10.1016/j.advwatres.2020.103682

Amrhein, V., Greenland, S., McShane, B., 2019. Scientists rise up against statistical significance. Nature 567, 305–307. https://doi.org/10.1038/d41586-019-00857-9

Andrews, F., Guillaume, J., 2018. hydromad.

Australian Bureau of Meteorology, 2020. Australian Gridded Climate Data (AGCD) / AWAP ; v1.0.0 Snapshot (1900-01-01 to 2018-12-31) [WWW Document]. URL http://www.bom.gov.au/metadata/catalogue/19115/ANZCW0503900567 (accessed 8.25.21).

Bahramian, K., Nathan, R., Western, A.W., Ryu, D., 2022. Probabilistic Conditioning and Recalibration of an Event-Based Flood Forecasting Model Using Real-Time Streamflow Observations. American Society of Civil Engineers Accepted. https://doi.org/10.1061/(ASCE)HE.1943-5584.0002236

Bahramian, K., Nathan, R., Western, A.W., Ryu, D., 2021. Towards an ensemble-based short-term flood forecasting using an event-based flood model- incorporating catchment-average estimates of soil moisture. Journal of Hydrology 593, 125828. https://doi.org/10.1016/j.jhydrol.2020.125828

Ball, J., Babister, M., Nathan, R., Weeks, W., Weinmann, E., Retallick, M., Testoni, I. (Eds.), 2019a. Australian Rainfall and Runoff: A Guide to Flood Estimation. Commonwealth of Australia (Geoscience Australia).

Ball, J., Babister, M., Nathan, R., Weeks, W., Weinmann, E., Retallick, M., Testoni, I., 2019b. Book 4 Catchment simulation for design flood estimation, in: Australian Rainfall and Runoff. p. 86.

Barnett, T.P., Pierce, D.W., Hidalgo, H.G., Bonfils, C., Santer, B.D., Das, T., Bala, G., Wood, A.W., Nozawa, T., Mirin, A.A., Cayan, D.R., Dettinger, M.D., 2008. Human-Induced Changes in the Hydrology of the Western United States. Science 319, 1080–1083. https://doi.org/10.1126/science.1152538

Bates, B., Kundzewicz, Z.W., IPCC (Eds.), 2008. Climate change and water, IPCC Technical Paper; 6.

Bennett, B., Leonard, M., Deng, Y., Westra, S., 2018. An empirical investigation into the effect of antecedent precipitation on flood volume. Journal of Hydrology 567, 435–445. https://doi.org/10.1016/j.jhydrol.2018.10.025

Berg, A., Sheffield, J., Milly, P.C.D., 2017. Divergent surface and total soil moisture projections under global warming. Geophysical Research Letters 44, 236–244. https://doi.org/10.1002/2016GL071921

Berthet, L., Andréassian, V., Perrin, C., Javelle, P., 2009. How crucial is it to account for the antecedent moisture conditions in flood forecasting? Comparison of event-based and continuous approaches on 178 catchments. Hydrol. Earth Syst. Sci. 13, 819–831. https://doi.org/10.5194/hess-13-819-2009

Blöschl, G., Gaál, L., Hall, J., Kiss, A., Komma, J., Nester, T., Parajka, J., Perdigão, R.A.P., Plavcová, L., Rogger, M., Salinas, J.L., Viglione, A., 2015. Increasing river floods: fiction or reality? WIREs Water 2, 329–344. https://doi.org/10.1002/wat2.1079

Brocca, L., Melone, F., Moramarco, T., Singh, V.P., 2009. Assimilation of Observed Soil Moisture Data in Storm Rainfall-Runoff Modeling. Journal of Hydrologic Engineering 14, 153–165. https://doi.org/10.1061/(ASCE)1084-0699(2009)14:2(153)

Bureau of Meteorology, 2020. Hydrologic Reference Stations: Station selection guidelines [WWW Document]. URL http://www.bom.gov.au/water/hrs/guidelines.shtml (accessed 10.21.21).

878 Camici, S., Brocca, L., Melone, F., Moramarco, T., 2014. Impact of Climate Change on Flood
879 Frequency Using Different Climate Models and Downscaling Approaches. Journal of
880 Hydrologic Engineering 19, 04014002. https://doi.org/10.1061/(ASCE)HE.1943-
881 5584.0000959
882 Camici, S., Tarpanelli, A., Brocca, L., Melone, F., Moramarco, T., 2011. Design soil moisture
883 estimation by comparing continuous and storm-based rainfall-runoff modeling.
884 Water Resources Research 47. https://doi.org/10.1029/2010WR009298
885 Chen, C., Haerter, J.O., Hagemann, S., Piani, C., 2011. On the contribution of statistical bias
886 correction to the uncertainty in the projected hydrological cycle. Geophys. Res. Lett.
887 38, L20403. https://doi.org/10.1029/2011gl049318
888 Cordery, I., 1970. Initial Loss for Flood Estimation and Forecasting. Journal of the Hydraulics
889 Division 96. https://doi.org/10.1061/JYCEAJ.0002794
890 Coustau, M., Ricci, S., Borrell-Estupina, V., Bouvier, C., Thual, O., 2013. Benefits and
891 limitations of data assimilation for discharge forecasting using an event-based
892 rainfall–runoff model. Natural Hazards and Earth System Sciences 13, 583–596.
893 https://doi.org/10.5194/nhess-13-583-2013
894 Department for Environment and Water, 2013. Natural Resource Management Regions.
895 Devineni, N., Lall, U., Pederson, N., Cook, E., 2013. A Tree-Ring-Based Reconstruction of
896 Delaware River Basin Streamflow Using Hierarchical Bayesian Regression. Journal of
897 Climate 26, 4357–4374. https://doi.org/10.1175/JCLI-D-11-00675.1
898 Do, H.X., Westra, S., Leonard, M., 2017. A global-scale investigation of trends in annual
899 maximum streamflow. Journal of Hydrology 552, 28–43.
900 https://doi.org/10.1016/j.jhydrol.2017.06.015
901 Dowdy, A., 2019. Towards seamless predictions across scales for fire weather, in:
902 Proceedings for the 6th International Fire Behavior and Fuels Conference. Presented
903 at the Fire Behavior and Fuels Conference, International Association of Wildland Fire,
904 Missoula, Montana, USA, Sydney, NSW.
905 Duan, Q., Sorooshian, S., Gupta, V., 1992. Effective and efficient global optimization for
906 conceptual rainfall-runoff models. Water Resources Research 28, 1015–1031.
907 https://doi.org/10.1029/91WR02985
908 Eagleson, P.S., 1972. Dynamics of flood frequency. Water Resources Research 8, 878–898.
909 https://doi.org/10.1029/WR008i004p00878
910 Eckhardt, K., 2008. A comparison of baseflow indices, which were calculated with seven
911 different baseflow separation methods. Journal of Hydrology 352, 168–173.
912 https://doi.org/10.1016/j.jhydrol.2008.01.005
913 Evans, A., Jones, D., Smalley, R., Lellyett, S., 2020. An enhanced gridded rainfall analysis
914 scheme for Australia (Bureau Research Report No. BRR041). Bureau of Meteorology.
915 Fowler, H.J., Lenderink, G., Prein, A.F., Westra, S., Allan, R.P., Ban, N., Barbero, R., Berg, P.,
916 Blenkinsop, S., Do, H.X., Guerreiro, S., Haerter, J.O., Kendon, E.J., Lewis, E., Schaer,
917 C., Sharma, A., Villarini, G., Wasko, C., Zhang, X., 2021. Anthropogenic intensification
918 of short-duration rainfall extremes. Nat Rev Earth Environ 2, 107–122.
919 https://doi.org/10.1038/s43017-020-00128-6
920 Frost, A.J., Ramchurn, A., Smith, A., 2018. The Australian Landscape Water Balance model
921 (AWRA-L v6): Technical Description of the Australian Water Resources Assessment
922 Landscape model version 6, Bureau of Meteorology Technical Report. Bureau of
923 Meteorology, Melbourne.

924 Frost, A.J., Shokri, A., Keir, G., Bahramian, K., Azarnivand, A., 2020. Evaluation of the
925 Australian Landscape Water Balance model (AWRA-L v7) (Bureau of Meteorology
926 Technical Report).
927 Grant, I., Jones, D., Wang, W., Fawcett, R., Barratt, D., 2008. Meteorological and Remotely
928 Sensed Datasets for Hydrological Modelling: A Contribution to the Australian Water
929 Availability Project, in: Proceedings of the Catchment-Scale Hydrological Modelling &
930 Data Assimilation (CAHMDA-3). Presented at the International Workshop on
931 Hydrological Prediction: Modelling, Observation and Data Assimilation, Melbourne.
932 Grose, M.R., Narsey, S., Delage, F.P., Dowdy, A.J., Bador, M., Boschat, G., Chung, C., Kajtar,
933 J.B., Rauniyar, S., Freund, M.B., Lyu, K., Rashid, H., Zhang, X., Wales, S., Trenham, C.,
934 Holbrook, N.J., Cowan, T., Alexander, L., Arblaster, J.M., Power, S., 2020. Insights
935 From CMIP6 for Australia's Future Climate. Earth's Future 8, e2019EF001469.
936 https://doi.org/10.1029/2019EF001469
937 Hanel, M., Buishand, T.A., 2011. Analysis of precipitation extremes in an ensemble of
938 transient regional climate model simulations for the Rhine basin. Clim Dyn 36, 1135–
939 1153. https://doi.org/10.1007/s00382-010-0822-2
940 Hempel, S., Frieler, K., Warszawski, L., Schewe, J., Piontek, F., 2013. A trend-preserving bias
941 correction – the ISI-MIP approach. Earth System Dynamics 4, 219–236.
942 https://doi.org/10.5194/esd-4-219-2013
943 Heneker, T.M., Lambert, M.F., Kuczera, G., 2003. Overcoming the joint probability problem
944 associated with initial loss estimation in desgn flood estimation. Australasian Journal
945 of Water Resources 7, 101–109. https://doi.org/10.1080/13241583.2003.11465233
946 Henley, B.J., Peel, M.C., Nathan, R., King, A.D., Ukkola, A.M., Karoly, D.J., Tan, K.S., 2019.
947 Amplification of risks to water supply at 1.5 °C and 2 °C in drying climates: a case
948 study for Melbourne, Australia. Environ. Res. Lett. 14, 084028.
949 https://doi.org/10.1088/1748-9326/ab26ef
950 Hijmans, R.J., van Etten, J., 2021. raster: Geographic data analysis and modeling.
951 Hill, P., Thomson, R., 2019. Chapter 3. Losses, in: Ball, J., Babister, M., Nathan, R., Weeks,
952 W., Weinmann, E., Retallick, M., Testoni, I. (Eds.), Book 5 Flood Hydrograph
953 Estimation, Australian Rainfall and Runoff: A Guide to Flood Estimation.
954 Ho, M., Lall, U., Sun, X., Cook, E.R.E.R., 2017. Multiscale temporal variability and regional
955 patterns in 555 years of conterminous U.S. streamflow. Water Resources Research
956 53. https://doi.org/10.1002/2016WR019632
957 Ho, M., Nathan, R., Wasko, C., Vogel, E., Sharma, A., 2022. Projecting changes in flood event
958 runoff coefficients under climate change. Journal of Hydrology accepted.
959 Holgate, C.M., De Jeu, R.A.M., van Dijk, A.I.J.M., Liu, Y.Y., Renzullo, L.J., Vinodkumar, Dharssi,
960 I., Parinussa, R.M., Van Der Schalie, R., Gevaert, A., Walker, J., McJannet, D., Cleverly,
961 J., Haverd, V., Trudinger, C.M., Briggs, P.R., 2016. Comparison of remotely sensed
962 and modelled soil moisture data sets across Australia. Remote Sensing of
963 Environment 186, 479–500. https://doi.org/10.1016/j.rse.2016.09.015
964 Institute of Hydrology, 1999. Flood Estimation Handbook (five volumes). Institute of
965 Hydrology, Oxfordshire, UK.
966 IPCC, 2021. Climate Change 2021: The Physical Science Basis. Cambridge University Press.
967 Ishak, E.H., Rahman, A., Westra, S., Sharma, A., Kuczera, G., 2013. Evaluating the non-
968 stationarity of Australian annual maximum flood. Journal of Hydrology 494, 134–145.
969 https://doi.org/10.1016/j.jhydrol.2013.04.021

970 Ivancic, T.J., Shaw, S.B., 2015. Examining why trends in very heavy precipitation should not
971 be mistaken for trends in very high river discharge. Climatic Change 133, 681–693.
972 https://doi.org/10.1007/s10584-015-1476-1
973 Johnson, F., White, C.J., van Dijk, A., Ekstrom, M., Evans, J.P., Jakob, D., Kiem, A.S., Leonard,
974 M., Rouillard, A., Westra, S., 2016. Natural hazards in Australia: floods. Climatic
975 Change 139, 21–35. https://doi.org/10.1007/s10584-016-1689-y
976 Jones, D., Wang, W., Fawcett, R., 2009. High-quality spatial climate data-sets for Australia.
977 AMOJ 58, 233–248. https://doi.org/10.22499/2.5804.003
978 Kiem, A.S., Verdon-Kidd, D.C., Austin, E.K., 2014. Bridging the gap between end user needs
979 and science capability: decision making under uncertainty. Climate Research 61, 57–
980 74. https://doi.org/10.3354/cr01243
981 Kim, S., Eghdamirad, S., Sharma, A., Kim, J.H., 2020. Quantification of Uncertainty in
982 Projections of Extreme Daily Precipitation. Earth and Space Science 7,
983 e2019EA001052. https://doi.org/10.1029/2019EA001052
984 Kjeldsen, T.R., 2007. Flood Estimation Handbook Supplementary Report No. 1, in: The
985 Revitalised FSR/FEH Rainfall-Runoff Method. Centre for Ecology and Hydrology, p.
986 68.
987 Krysanova, V., White, M., 2015. Advances in water resources assessment with SWAT—an
988 overview. Hydrological Sciences Journal 60, 771–783.
989 https://doi.org/10.1080/02626667.2015.1029482
990 Kuczera, G., Lambert, M., Heneker, T., Jennings, S., Frost, A., Coombes, P., 2006. Joint
991 probability and design storms at the crossroads. Australasian Journal of Water
992 Resources 10, 63–79. https://doi.org/10.1080/13241583.2006.11465282
993 Kunkel, K.E., Schlef, K., Brown, C., François, B., Demissie, Y., Yan, E., Lettenmaier, D.P., Wang,
994 K.J., Wagner, A., Wigmosta, M.S., Karl, T.R., Easterling, D.R., 2020. Best Practices for
995 Incorporating Non-stationarity in Extreme Precipitation and Flooding Design Values
996 (SERDP Best Practices Manual No. RC-2517). Virginia, US.
997 Kwon, H.-H., Sivakumar, B., Moon, Y.-I., Kim, B.-S., 2011. Assessment of change in design
998 flood frequency under climate change using a multivariate downscaling model and a
999 precipitation-runoff model. Stoch Environ Res Risk Assess 25, 567–581.
1000 https://doi.org/10.1007/s00477-010-0422-z
1001 Ladson, A., Brown, R., Neal, B., Nathan, R., 2013. A standard approach to baseflow
1002 separation using the Lyne and Hollick filter. AJWR 17. https://doi.org/10.7158/W12-
1003 028.2013.17.1
1004 Lang, M., Ouarda, T.B.M.J., Bobée, B., 1999. Towards operational guidelines for over-
1005 threshold modeling. Journal of Hydrology 225, 103–117.
1006 https://doi.org/10.1016/S0022-1694(99)00167-5
1007 Lenderink, G., van Meijgaard, E., 2008. Increase in hourly precipitation extremes beyond
1008 expectations from temperature changes. Nature Geoscience 1, 511–514.
1009 https://doi.org/10.1038/ngeo262
1010 Lettenmaier, D.P., Wood, E.F., 1993. Chapter 26 Hydrologic Forecasting, in: Maidment, D.R.
1011 (Ed.), Handbook of Hydrology. McGraw-Hill, New York.
1012 Li, J., Thyer, M., Lambert, M., Kuczera, G., Metcalfe, A., 2014. An efficient causative event-
1013 based approach for deriving the annual flood frequency distribution. Journal of
1014 Hydrology 510, 412–423. https://doi.org/10.1016/j.jhydrol.2013.12.035
1015 Lins, H.F., Slack, J.R., 1999. Streamflow trends in the United States. Geophysical Research
1016 Letters 26, 227–230. https://doi.org/10.1029/1998GL900291

Liu, S.C., Fu, C., Shiu, C.-J., Chen, J.-P., Wu, F., 2009. Temperature dependence of global precipitation extremes. Geophysical Research Letters 36. https://doi.org/10.1029/2009GL040218

Lyne, V., Hollick, M., 1979. Stochastic time-variable rainfall-runoff modelling, in: Institution of Engineers National Conference Publication. Presented at the Proceedings of the Hydrology and Water Resources Symposium, Perth, pp. 89–92.

Madsen, H., Lawrence, D., Lang, M., Martinkova, M., Kjeldsen, T.R., 2014. Review of trend analysis and climate change projections of extreme precipitation and floods in Europe. Journal of Hydrology 519, 3634–3650. https://doi.org/10.1016/j.jhydrol.2014.11.003

Markham, C.G., 1970. Seasonality of Precipitation in the United States. Annals of the Association of American Geographers 60, 593–597. https://doi.org/10.1111/j.1467-8306.1970.tb00743.x

Mcgregor, J.L., Dix, M.R., 2001. The CSIRO Conformal-Cubic Atmospheric GCM, in: Hodnett, P.F. (Ed.), IUTAM Symposium on Advances in Mathematical Modelling of Atmosphere and Ocean Dynamics. Springer Netherlands, Dordrecht, pp. 197–202. https://doi.org/10.1007/978-94-010-0792-4_25

McKenzie, N., Jacquier, D., Gregory, L., Cresswell, H., 2000. Estimation of Soil Properties Using the Atlas of Australian Soils.

McVicar, T.R., Van Niel, T.G., Li, L.T., Roderick, M.L., Rayner, D.P., Ricciardulli, L., Donohue, R.J., 2008. Wind speed climatology and trends for Australia, 1975–2006: Capturing the stilling phenomenon and comparison with near-surface reanalysis output. Geophysical Research Letters 35. https://doi.org/10.1029/2008GL035627

Mehrotra, R., Johnson, F., Sharma, A., 2018. A software toolkit for correcting systematic biases in climate model simulations. Environmental Modelling & Software 104, 130–152. https://doi.org/10.1016/j.envsoft.2018.02.010

Mehrotra, R., Sharma, A., 2015. Correcting for systematic biases in multiple raw GCM variables across a range of timescales. Journal of Hydrology 520, 214–223. https://doi.org/10.1016/j.jhydrol.2014.11.037

Mein, R.G., Nandakumar, N., Siriwardena, L., 1995. Estimation of initial loss from soil moisture indices (Pilot Study) (No. Working Document 95/1). Cooperative Research Centre for Catchment Hydrology.

Meinshausen, M., Smith, S.J., Calvin, K., Daniel, J.S., Kainuma, M.L.T., Lamarque, J.-F., Matsumoto, K., Montzka, S.A., Raper, S.C.B., Riahi, K., Thomson, A., Velders, G.J.M., van Vuuren, D.P.P., 2011. The RCP greenhouse gas concentrations and their extensions from 1765 to 2300. Climatic Change 109, 213. https://doi.org/10.1007/s10584-011-0156-z

Moise, A., Bhend, J., Watterson, I., Wilson, L., 2015. Evaluation of Climate Models, in: Whetton, P., Ekström, M., Gerbing, C., Grose, M.R., Bhend, J., Webb, L., Risbey, J. (Eds.), Climate Change in Australia Information for Australia's Natural Resource Mangaement Regions: Technical Report. pp. 53–76.

Murphy, R., Graszkiewicz, Z., Hill, P., Neal, B., Nathan, R., Ladson, T., 2009. Australia Rainfall and Runoff Revision Project 7: Baseflow for Catchment Simulation - Selection Approach (No. P7/S1/004). Engineers Australia, Barton, ACT.

Nathan, R.J., McMahon, T.A., 1990. Evaluation of automated techniques for base flow and recession analyses. Water Resources Research 26, 1465–1473. https://doi.org/10.1029/WR026i007p01465

Nathan, R.J., Weinmann, P.E., Hill, P.I., 2002. Use of a Monte Carlo framework to characterise hydrologic risk. ANCOLD 55–64.
Nese, J.M., Grenci, L.M., 2005. A world of weather: fundamentals of meteorology. Kendall/Hunt Publishing Co, USA.
Nguyen, H., Mehrotra, R., Sharma, A., 2020. Assessment of Climate Change Impacts on Reservoir Storage Reliability, Resilience, and Vulnerability Using a Multivariate Frequency Bias Correction Approach. Water Resources Research 56, e2019WR026022. https://doi.org/10.1029/2019WR026022
O'Shea, D., Nathan, R., Wasko, C., Hill, P., 2021. Implications of event-based loss model structure on simulating large floods. Journal of Hydrology 595, 126008. https://doi.org/10.1016/j.jhydrol.2021.126008
Pan, X., Rahman, A., Haddad, K., Ouarda, T.B.M.J., 2022. Peaks-over-threshold model in flood frequency analysis: a scoping review. Stoch Environ Res Risk Assess 36, 2419–2435. https://doi.org/10.1007/s00477-022-02174-6
Papalexiou, S.M., Montanari, A., 2019. Global and Regional Increase of Precipitation Extremes under Global Warming. Water Resources Research 0. https://doi.org/10.1029/2018WR024067
Paquet, E., Garavaglia, F., Garçon, R., Gailhard, J., 2013. The SCHADEX method: A semi-continuous rainfall–runoff simulation for extreme flood estimation. Journal of Hydrology 495, 23–37. https://doi.org/10.1016/j.jhydrol.2013.04.045
Pathiraja, S., Westra, S., Sharma, A., 2012. Why continuous simulation? The role of antecedent moisture in design flood estimation. Water Resources Research 48. https://doi.org/10.1029/2011WR010997
Peel, M.C., Finlayson, B.L., McMahon, T.A., 2007. Updated world map of the Köppen-Geiger climate classification. Hydrology and Earth System Sciences 11, 1633–1644. https://doi.org/10.5194/hess-11-1633-2007
Peleg, N., Marra, F., Fatichi, S., Molnar, P., Morin, E., Sharma, A., Burlando, P., 2018. Intensification of Convective Rain Cells at Warmer Temperatures Observed from High-Resolution Weather Radar Data. Journal of Hydrometeorology 19, 715–726. https://doi.org/10.1175/JHM-D-17-0158.1
Perrin, C., Michel, C., Andréassian, V., 2003. Improvement of a parsimonious model for streamflow simulation. Journal of Hydrology 279, 275–289. https://doi.org/10.1016/S0022-1694(03)00225-7
Pilgrim, D., 1987. Australian Rainfall and Runoff: A Guide to Flood Estimation. Institute of Engineers Australia, Barton, Australia.
Pilgrim, D.H., Cordery, I., 1993. Chapter 9 - Flood Runoff', in: Maidment, D.R. (Ed.), Handbook of Hydrology. McGraw-Hill, New York.
Priestley, M.D.K., Catto, J.L., 2022. Future changes in the extratropical storm tracks and cyclone intensity, wind speed, and structure. Weather and Climate Dynamics 3, 337–360. https://doi.org/10.5194/wcd-3-337-2022
Prudhomme, C., Reynard, N., Crooks, S., 2002. Downscaling of global climate models for flood frequency analysis: where are we now? Hydrological Processes 16, 1137–1150. https://doi.org/10.1002/hyp.1054
Rahman, A., Weinmann, P.E., Hoang, T.M.T., Laurenson, E.M., 2002. Monte Carlo simulation of flood frequency curves from rainfall. Journal of Hydrology 256, 196–210. https://doi.org/10.1016/S0022-1694(01)00533-9

Saul, A.J., 1997. Chapter 8 - Hydraulic Assessment, in: Read, G.F., Vickridge, I.G. (Eds.), Sewers. Butterworth-Heinemann, London, pp. 149–192. https://doi.org/10.1016/B978-034054472-3/50011-8

Seneviratne, S.I., Corti, T., Davin, E.L., Hirschi, M., Jaeger, E.B., Lehner, I., Orlowsky, B., Teuling, A.J., 2010. Investigating soil moisture–climate interactions in a changing climate: A review. Earth-Science Reviews 99, 125–161. https://doi.org/10.1016/j.earscirev.2010.02.004

Sharma, A., Wasko, C., Lettenmaier, D.P., 2018. If Precipitation Extremes Are Increasing, Why Aren't Floods? Water Resources Research 54, 8545–8551. https://doi.org/10.1029/2018WR023749

Sheikh, V., Visser, S., Stroosnijder, L., 2009. A simple model to predict soil moisture: Bridging Event and Continuous Hydrological (BEACH) modelling. Environmental Modelling & Software 24, 542–556. https://doi.org/10.1016/j.envsoft.2008.10.005

Sloto, R.A., Crouse, M.Y., 1996. HYSEP: A Computer Program for Streamflow Hydrograph Separation and Analysis (No. 90–4040), Water-Resources Investigations Report. Denver, CO. https://doi.org/10.3133/wri964040

Smith, J.A., Baeck, M.L., Villarini, G., Wright, D.B., Krajewski, W., 2013. Extreme Flood Response: The June 2008 Flooding in Iowa. Journal of Hydrometeorology 14, 1810–1825. https://doi.org/10.1175/JHM-D-12-0191.1

Srikanthan, S., Bende-Michl, U., Wilson, L., Sharples, W., Vogel, E., Peter, J.R., Hope, P.K., Loh, S., Khan, Z., Duong, V., Roussis, J., Dowdy, A., Oke, A., Matic, V., Turner, M., Kociuba, G., Thomas, S., Azarnivand, A., Donnelly, C., Carrara, E., 2022. National Hydrological Projections - Design and Methodology (No. BRR061), Bureau Research Report. Bureau of Meteorology.

Stephens, C.M., Johnson, F.M., Marshall, L.A., 2018. Implications of future climate change for event-based hydrologic models. Advances in Water Resources 119, 95–110. https://doi.org/10.1016/j.advwatres.2018.07.004

Strupczewski, W.G., Singh, V.P., Feluch, W., 2001. Non-stationary approach to at-site flood frequency modelling I. Maximum likelihood estimation. Journal of Hydrology 248, 123–142. https://doi.org/10.1016/S0022-1694(01)00397-3

Sturman, A.P., Tapper, N.J., 1996. The weather and climate of Australia and New Zealand. Oxford University Press, USA.

Sun, X., Lall, U., Merz, B., Dung, N.V., 2015. Hierarchical Bayesian clustering for nonstationary flood frequency analysis: Application to trends of annual maximum flow in Germany. Water Resources Research 51, 6586–6601. https://doi.org/10.1002/2015WR017117

Sunwoo, W., Choi, M., 2017. Robust Initial Wetness Condition Framework of an Event-Based Rainfall–Runoff Model Using Remotely Sensed Soil Moisture. Water 9, 77. https://doi.org/10.3390/w9020077

Suppiah, R., 1992. The Australian summer monsoon: a review. Progress in Physical Geography: Earth and Environment 16, 283–318. https://doi.org/10.1177/030913339201600302

Tramblay, Y., Bouvier, C., Martin, C., Didon-Lescot, J.-F., Todorovik, D., Domergue, J.-M., 2010. Assessment of initial soil moisture conditions for event-based rainfall–runoff modelling. Journal of Hydrology 387, 176–187. https://doi.org/10.1016/j.jhydrol.2010.04.006

Tramblay, Y., Villarini, G., El Khalki, E.M., Gründemann, G., Hughes, D., 2021. Evaluation of the Drivers Responsible for Flooding in Africa. Water Resources Research 57, e2021WR029595. https://doi.org/10.1029/2021WR029595

Trenberth, K.E., 2011. Changes in precipitation with climate change. Climate Research 47, 123–138. https://doi.org/10.3354/cr00953

Trenberth, K.E., 1999. Conceptual Framework for Changes of Extremes of the Hydrological Cycle With Climate Change, in: Karl, T.R., Nicholls, N., Ghazi, A. (Eds.), Weather and Climate Extremes: Changes, Variations and a Perspective from the Insurance Industry. Springer Netherlands, Dordrecht, pp. 327–339. https://doi.org/10.1007/978-94-015-9265-9_18

United States Department of Agriculture (Ed.), 2014. Chapter 17 Flood Routing, in: National Engineering Handbook. Washington, D. C., USA.

US Army Corps of Engineers, 2000. HEC-HMS Technical Reference Manual.

Utsumi, N., Kim, H., 2022. Observed influence of anthropogenic climate change on tropical cyclone heavy rainfall. Nat. Clim. Chang. 12, 436–440. https://doi.org/10.1038/s41558-022-01344-2

van Vuuren, D.P., Edmonds, J., Kainuma, M., Riahi, K., Thomson, A., Hibbard, K., Hurtt, G.C., Kram, T., Krey, V., Lamarque, J.-F., Masui, T., Meinshausen, M., Nakicenovic, N., Smith, S.J., Rose, S.K., 2011. The representative concentration pathways: an overview. Climatic Change 109, 5. https://doi.org/10.1007/s10584-011-0148-z

Visser, J.B., Wasko, C., Sharma, A., Nathan, R., submitted to Journal of Climate. Are temporal patterns of precipitation changing in a warming climate? Journal of Climate.

Wang, G.Q., Zhang, J.Y., Jin, J.L., Pagano, T.C., Calow, R., Bao, Z.X., Liu, C.S., Liu, Y.L., Yan, X.L., 2012. Assessing water resources in China using PRECIS projections and a VIC model. Hydrology and Earth System Sciences 16, 231–240. https://doi.org/10.5194/hess-16-231-2012

Wang, J., Kotamarthi, V.R., 2015. High-resolution dynamically downscaled projections of precipitation in the mid and late 21st century over North America. Earth's Future 3, 268–288. https://doi.org/10.1002/2015EF000304

Wasko, C., Guo, D., 2022. Understanding event runoff coefficient variability across Australia using the hydroEvents R package. Hydrological Processes 36, e14563. https://doi.org/10.1002/hyp.14563

Wasko, C., Guo, D., Ho, M., Nathan, R., Vogel, E., 2023. Diverging projections for flood and rainfall frequency curves. Journal of Hydrology 620, 129403. https://doi.org/10.1016/j.jhydrol.2023.129403

Wasko, C., Nathan, R., 2019. Influence of changes in rainfall and soil moisture on trends in flooding. Journal of Hydrology 575, 432–441. https://doi.org/10.1016/j.jhydrol.2019.05.054

Wasko, C., Nathan, R., Peel, M.C., 2020. Changes in Antecedent Soil Moisture Modulate Flood Seasonality in a Changing Climate. Water Resources Research 56, e2019WR026300. https://doi.org/10.1029/2019WR026300

Wasko, C., Nathan, R., Stein, L., O'Shea, D., 2021a. Evidence of shorter more extreme rainfalls and increased flood variability under climate change. Journal of Hydrology 603, 126994. https://doi.org/10.1016/j.jhydrol.2021.126994

Wasko, C., Sharma, A., Westra, S., 2016. Reduced spatial extent of extreme storms at higher temperatures. Geophysical Research Letters 43, 4026–4032. https://doi.org/10.1002/2016GL068509

Wasko, C., Westra, S., Nathan, R., Orr, H.G., Villarini, G., Villalobos Herrera, R., Fowler, H.J., 2021b. Incorporating climate change in flood estimation guidance. Philosophical Transactions of the Royal Society A: Mathematical, Physical and Engineering Sciences 379, 20190548. https://doi.org/10.1098/rsta.2019.0548

Westra, S., Fowler, H.J., Evans, J.P., Alexander, L.V., Berg, P., Johnson, F., Kendon, E.J., Lenderink, G., Roberts, N.M., 2014. Future changes to the intensity and frequency of short-duration extreme rainfall. Reviews of Geophysics 52, 522–555. https://doi.org/10.1002/2014RG000464

Wheeler, M.C., Hendon, H.H., Cleland, S., Meinke, H., Donald, A., 2009. Impacts of the Madden–Julian Oscillation on Australian Rainfall and Circulation. Journal of Climate 22, 1482–1498. https://doi.org/10.1175/2008JCLI2595.1

Wilson, L., Bende-Michl, U., Sharples, W., Vogel, E., Peter, J., Srikanthan, S., Khan, Z., Matic, V., Oke, A., Turner, M., Co Duong, V., Loh, S., Baron-Hay, S., Roussis, J., Kociuba, G., Hope, P., Dowdy, A., Donnelly, C., Argent, R., Thomas, S., Kitsios, A., Bellhouse, J., 2022. A national hydrological projections service for Australia. Climate Services 28, 100331. https://doi.org/10.1016/j.cliser.2022.100331

Woldemeskel, F., Sharma, A., 2016. Should flood regimes change in a warming climate? The role of antecedent moisture conditions. Geophysical Research Letters 43, 7556–7563. https://doi.org/10.1002/2016GL069448

Wright, D.B., Smith, J.A., Baeck, M.L., 2014. Flood frequency analysis using radar rainfall fields and stochastic storm transposition. Water Resources Research 50, 1592–1615. https://doi.org/10.1002/2013WR014224

Wright, P.B., 1974. Seasonal Rainfall in Southwestern Australia and the General Circulation. Monthly Weather Review 102, 219–232. https://doi.org/10.1175/1520-0493(1974)102<0219:SRISAA>2.0.CO;2

Yu, G., Wright, D.B., Zhu, Z., Smith, C., Holman, K.D., 2019. Process-based flood frequency analysis in an agricultural watershed exhibiting nonstationary flood seasonality. Hydrology and Earth System Sciences 23, 2225–2243. https://doi.org/10.5194/hess-23-2225-2019

Zhang, X.S., Amirthanathan, G.E., Bari, M.A., Laugesen, R.M., Shin, D., Kent, D.M., MacDonald, A.M., Turner, M.E., Tuteja, N.K., 2016. How streamflow has changed across Australia since the 1950s: evidence from the network of hydrologic reference stations. Hydrology and Earth System Sciences 20, 3947–3965. https://doi.org/10.5194/hess-20-3947-2016

Appendix

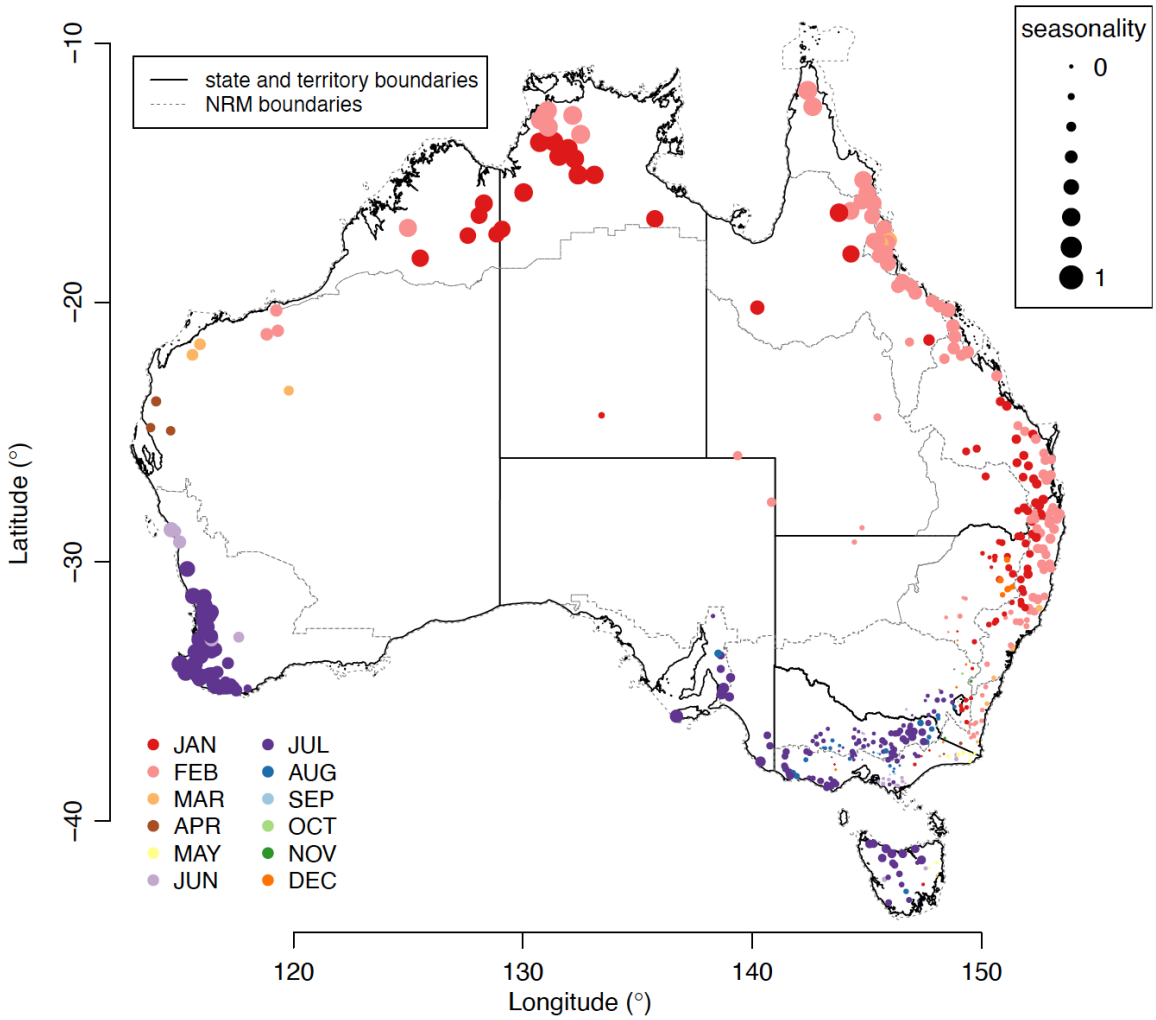

Figure A. 1. Seasonality of 3-day rainfall events larger than the 5 EY event. A value of 1 correspond to all events occurring within a single month and a value of 0 indicates an even distribution of events throughout the year

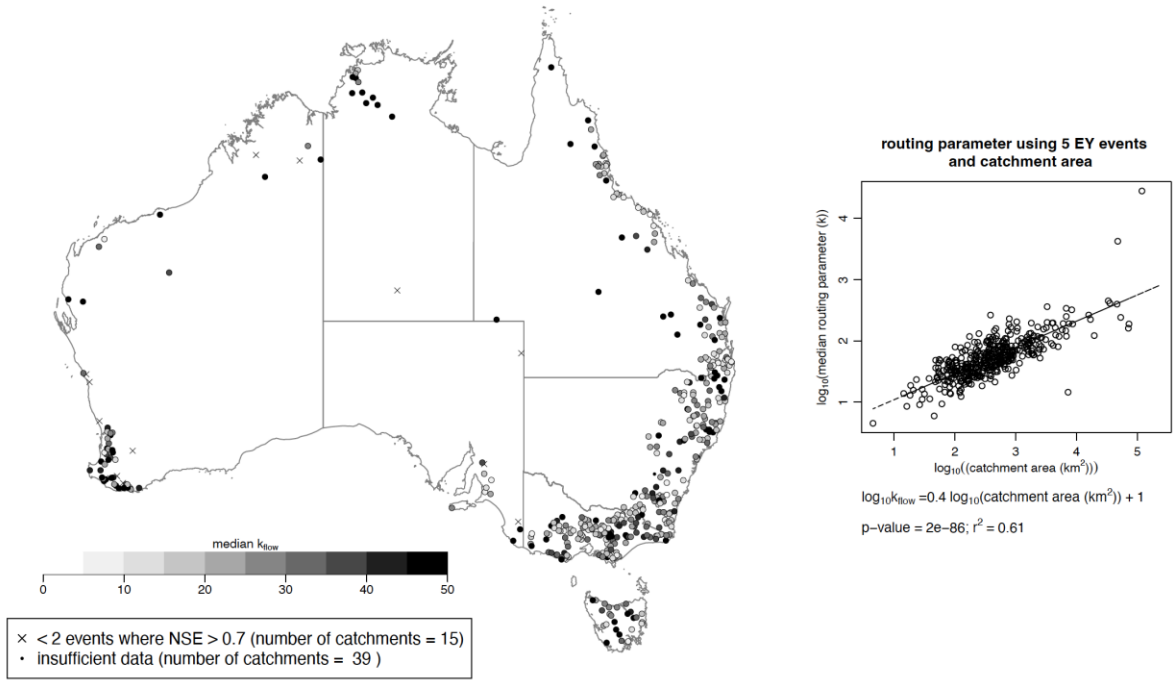

1242

1243 *Figure A. 2. Value of median routing parameter, k, calculated for catchments with sufficient hourly data for events*

1244 *containing 3-day rainfall events larger than the 5 EY and calibration of two or more events resulting in NSE > 0.7 (total of*

1245 *413 catchments) plotted as (left) a map and (right) plotted against the catchment area on a log_{10} scale.*

1246

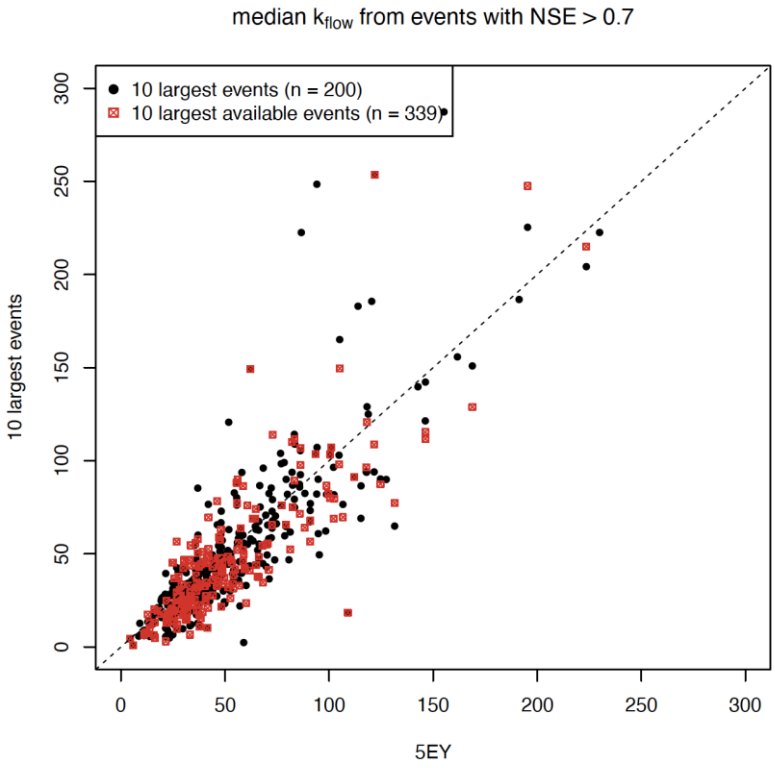

Figure A. 3. Median routing parameter, k, calculated from events containing 3-day rainfalls larger than the 5 EY event compared with values calculated using the rainfall and runoff events containing the 10 largest three-day rainfalls (black points - 200 catchments with sufficient data from these events) and 10 largest three-day rainfalls where both gauged streamflow and gauged rainfall data are available (red squares with sufficient data from 339 catchments).

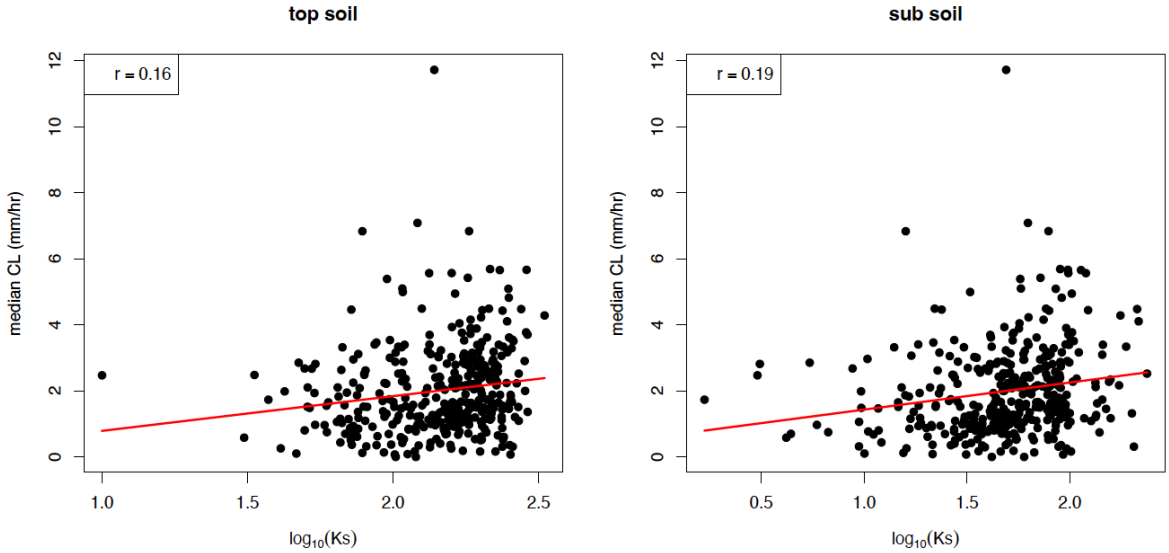

1252

1253 *Figure A. 4. Scatter plots of catchment-median continuing loss against log base 10 of the catchment (left) top soil hydraulic*

1254 *conductivity (K_s) and (right) sub soil hydraulic conductivity. Correlation coefficient with n=380 degrees of freedom shown in*

1255 *top left of each plot excluding catchments where K_s=0.*

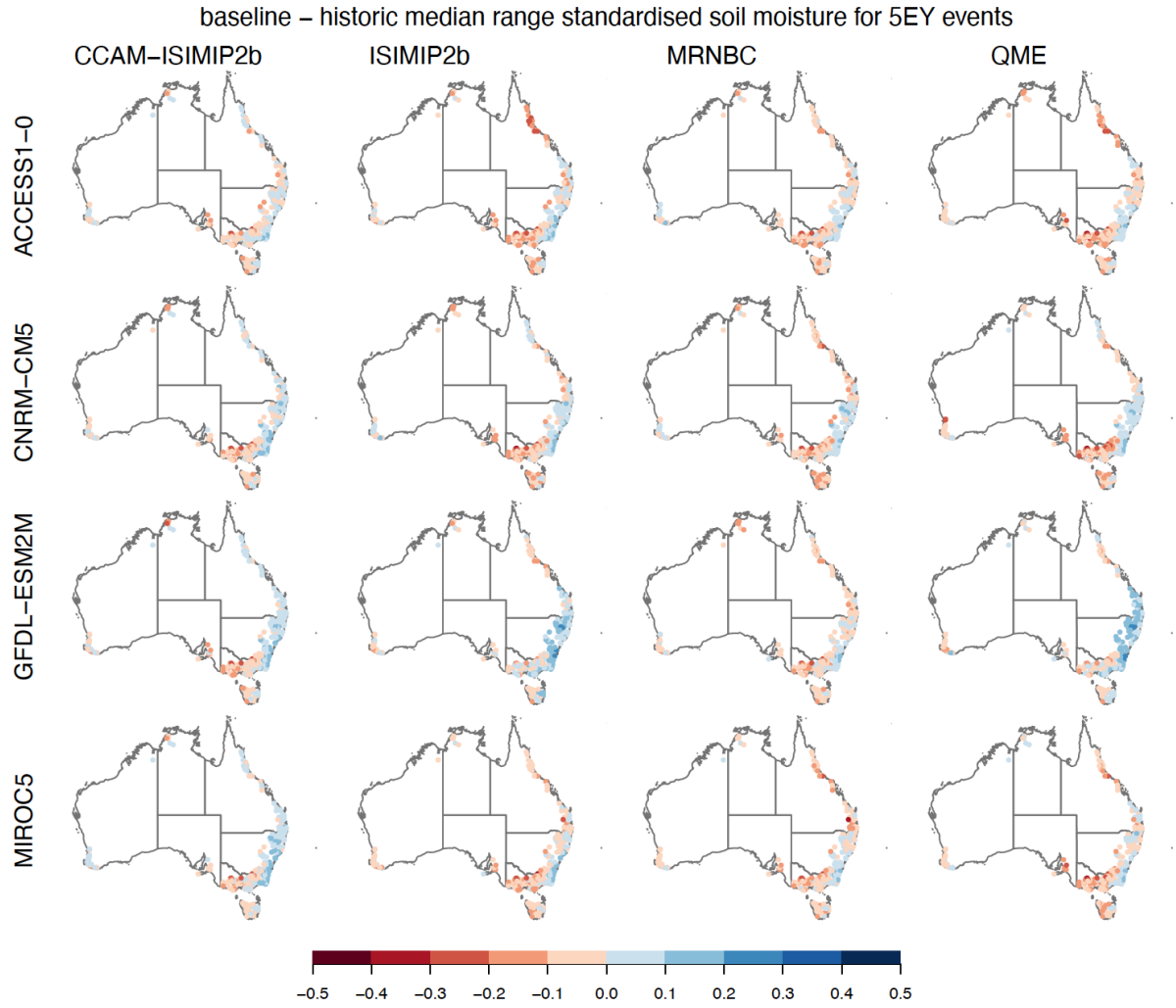

Figure A. 5. Difference between baseline and historic median soil moisture for 5EY events over the 1976-2005 period mapped for catchments where the slope of the linear regression between either initial loss or continuing loss and range-standardised soil moisture is significant at a level of $\alpha = 0.05$.

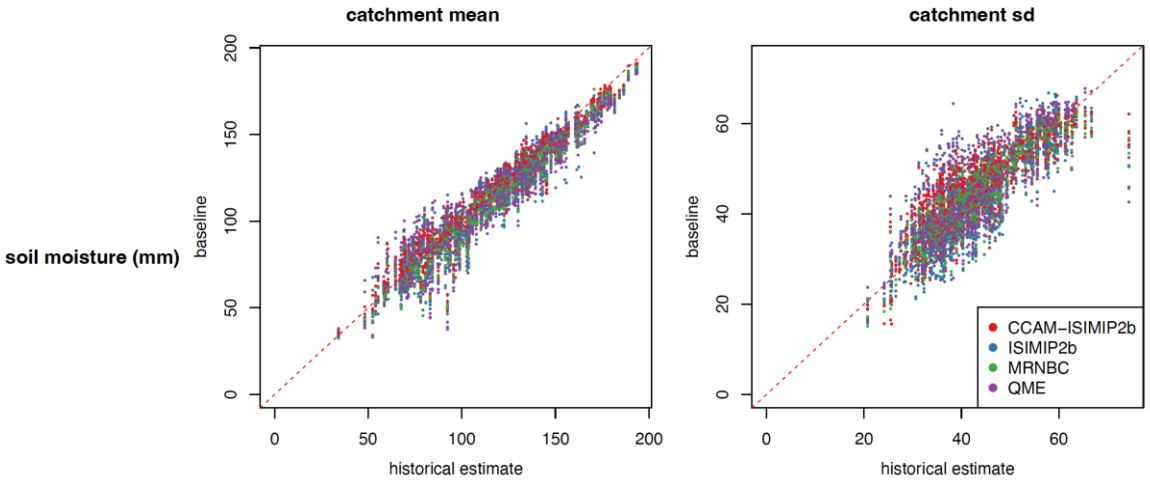

Figure A. 6. Catchment mean and standard deviation of soil moisture for 5EY events over the 1976-2005 period showing baseline soil moisture from the 16 member GCM ensemble against historic soil moisture for catchments where the slope of the linear regression between either initial loss or continuing loss and soil moisture is significant at a level of $\alpha = 0.05$.

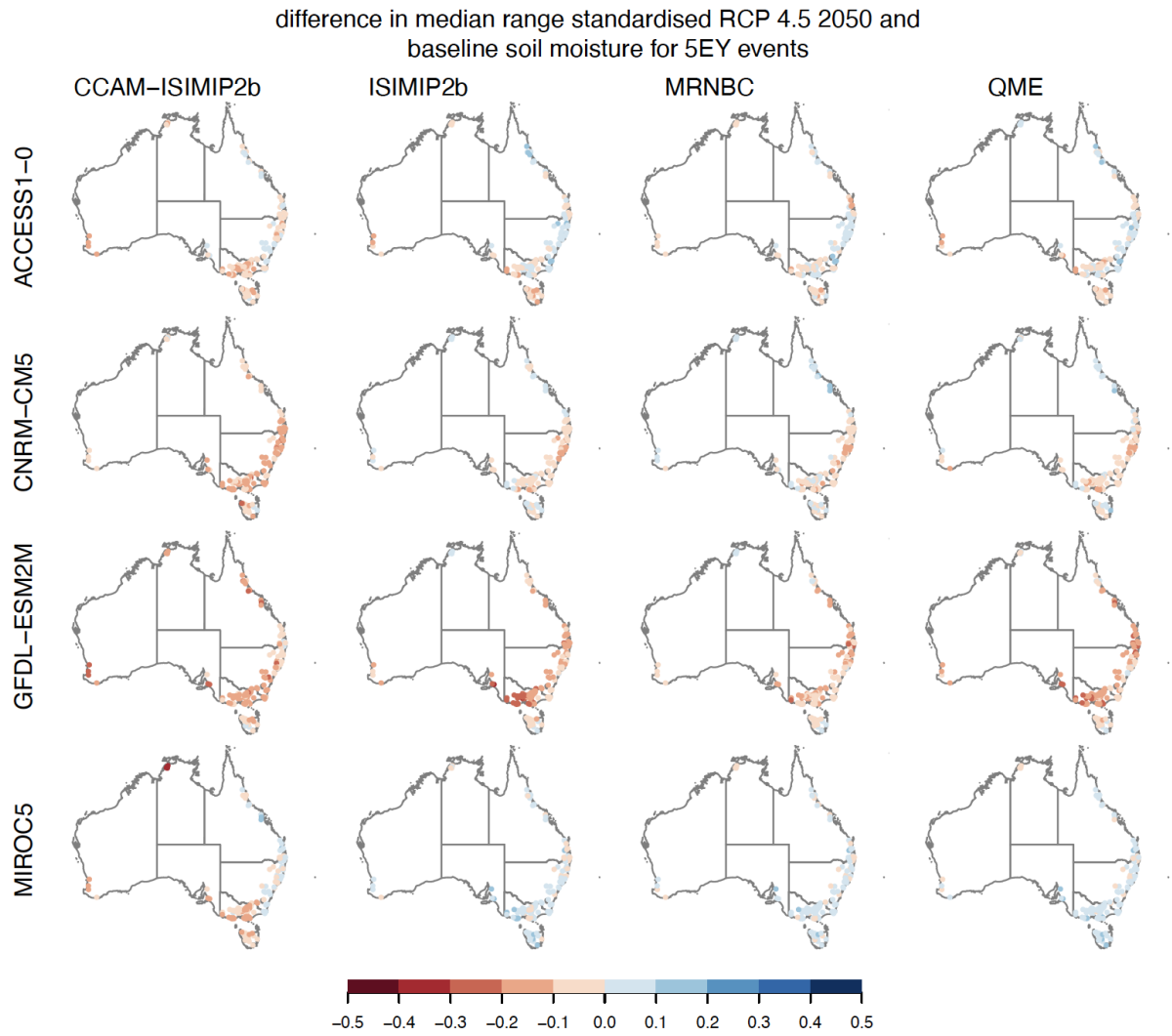

Figure A. 7. Projected changes in range standardised soil moisture from the baseline to RCP 4.5 scenario for the 30 years centred on 2050.

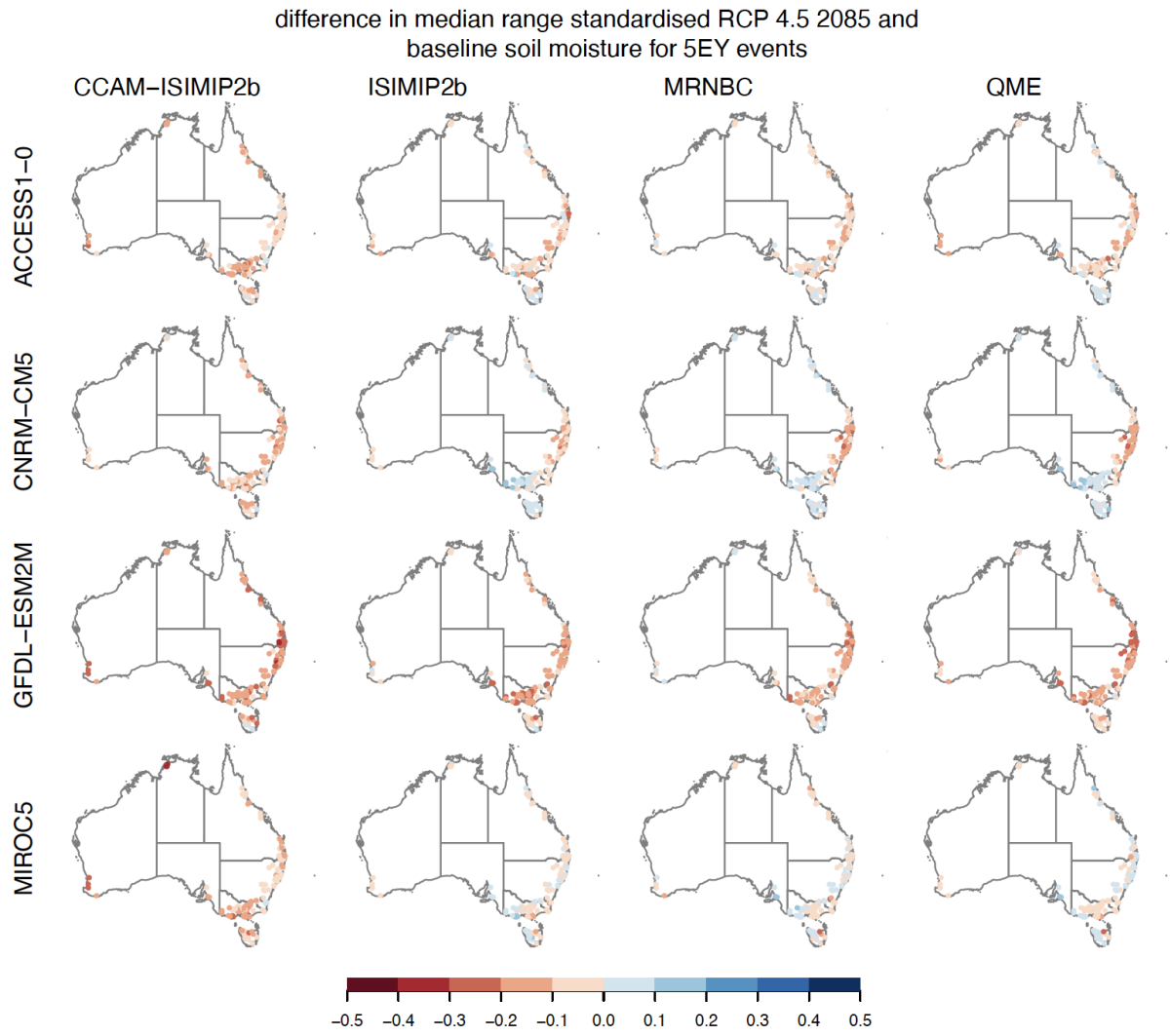

Figure A. 8. Projected changes in range standardised soil moisture from the baseline to RCP 4.5 scenario for the 30 years centred on 2085.

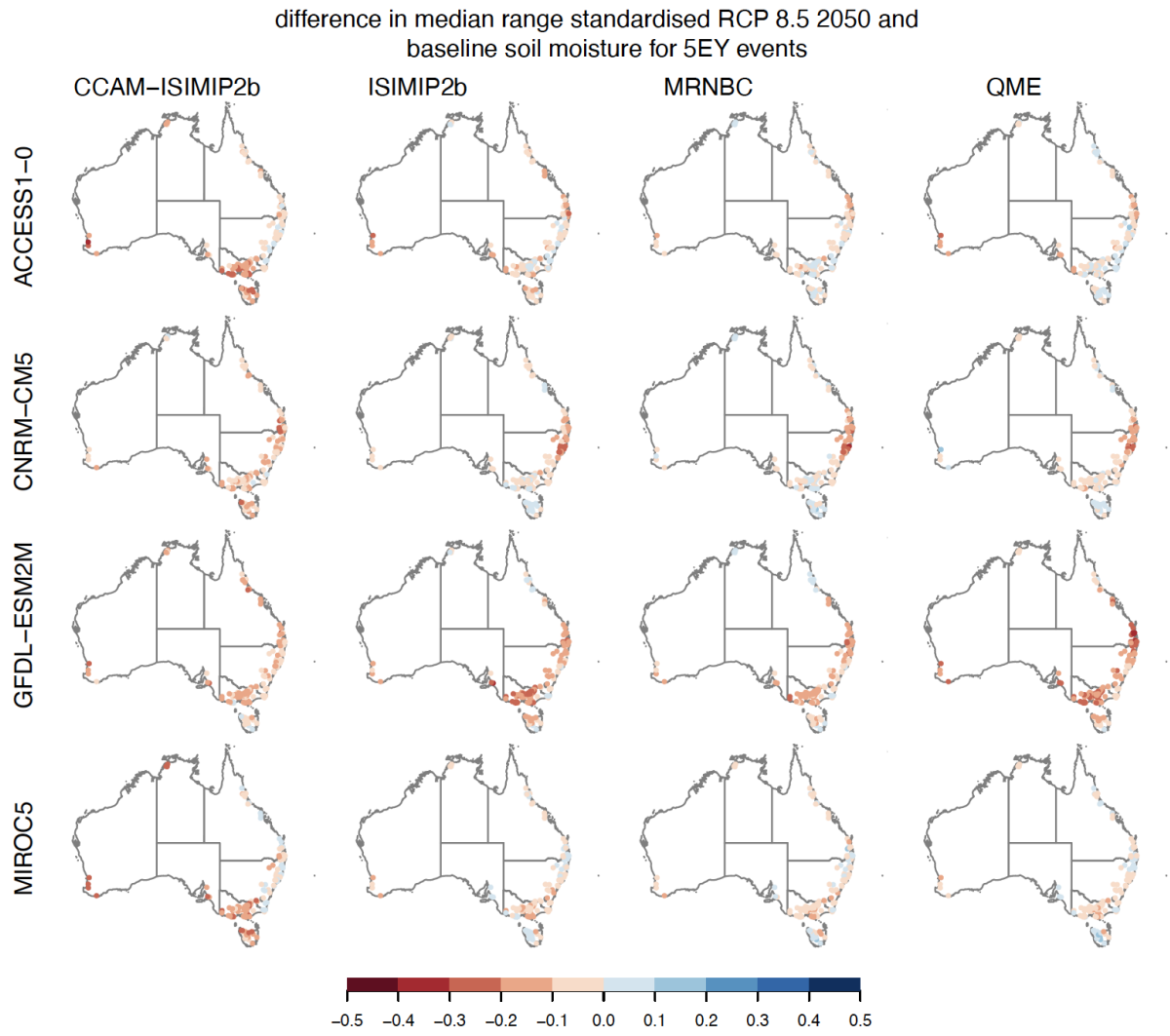

Figure A. 9. Projected changes in range standardised soil moisture from the baseline to RCP 8.5 scenario for the 30 years centred on 2050

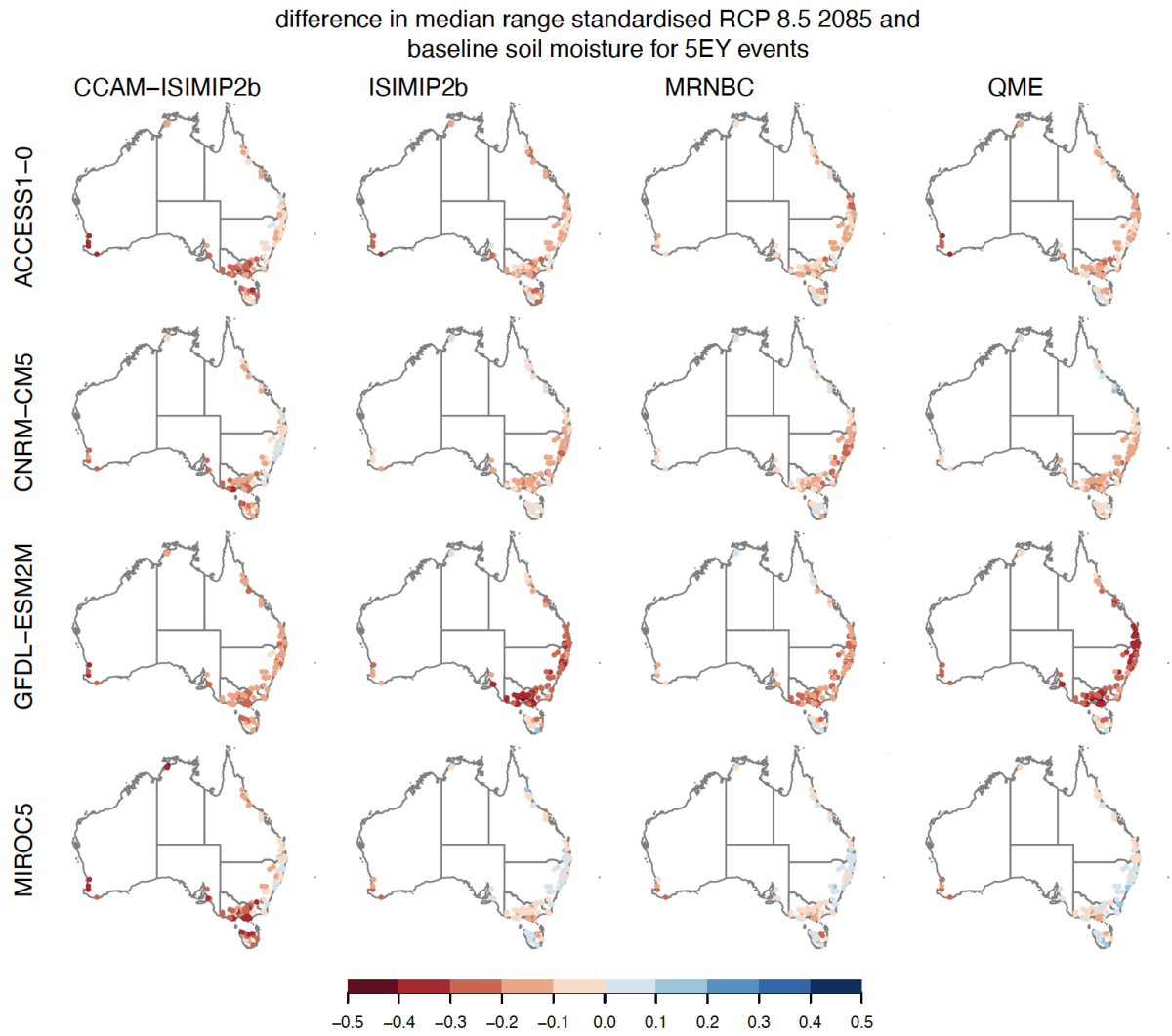

Figure A. 10. Projected changes in range standardised soil moisture from the baseline to RCP 8.5 scenario for the 30 years centred on 2085